Saturn
Developing Solutions for Underwater Radiated Noise

SATURN has received funding from the European Union's Horizon 2020 research and innovation programme under grant agreement No. 101006443.

SATURN Deliverable D2.2

Guidelines for sound particle motion mapping

Author(s): Christ de Jong, Bas Binnerts, Timo Gaida, Erwin Jansen (TNO)
Michael Ainslie, Michael Wood (JASCO)

PUBLIC

July 2024

Document Information

Document Details	
Grant Agreement Number	101006443
Project Acronym	SATURN
Work Package	WP2
Task(s)	T2.3
Deliverable	D2.2
Title	Guidelines for sound particle motion mapping
Authors	Christ de Jong et al. (see below)
File name	SATURN D2.2 Guidelines for sound particle motion mapping.docx
Delivery date	July 2024
Dissemination level	PUBLIC
Keywords	Underwater sound, particle motion, modelling, verification, validation

Version	Date	Description	Authors	Reviewed by	Approved by
1.0	28-3-2024	draft	CdJ et al	authors	CdJ
2.0	26-4-2024	Revised	CdJ et al	Niels Kinneging Peter Sigray Hans Slabbekoorn Dominique Clorennec & Julien Bellanger	
final	8-7-2024	Revised	CdJ et al		SATURN

Authors (alphabetical) and Organisation	
Bas Binnerts	TNO
Christ de Jong	TNO
Erwin Jansen	TNO
Michael Ainslie	JASCO
Michael Wood	JASCO
Timo Gaida	TNO

Acknowledgements/contributions (alphabetical)	
Name	Organisation
Eef Brouns & Mark van Spellen	TNO measurement team

Disclaimer

Table of Contents

Executive Summary

Models for mapping sound pressure metrics over the environment in which animals are exposed to underwater radiated noise from ships have been developed in previous projects and applied in European ambient sound monitoring projects such as BIAS, JOMOPANS and JONAS. However, these maps represent metrics based on sound pressure within set frequency ranges. The capability to produce maps of metrics based on sound particle motion, to which many fish and invertebrate species are sensitive, still needed to be developed.

This deliverable from Task 2.3 'Sound Particle Motion Modelling and Mapping' of the EU-funded research project SATURN (Developing solutions to underwater radiated noise) describes the results of the development of the capability to produce sound particle motion maps. It describes the relevant sound particle motion metrics and how these relate, describes models that can be used for producing sound particle motion maps, describes how these models can be verified and validated and provides some examples of calculated particle motion sound maps.

The final chapter of this report summarizes guidelines for sound particle motion mapping.

List of Abbreviations

AIS	Automatic Identification System of ships
FE	Finite element
IS	Image source
ISO	International organization for standardization
PAEL	Time-integrated squared radial sound particle acceleration level
PAL	Sound particle acceleration level
PE	Parabolic equation
PM	Sound particle motion
PVL	Sound particle velocity level
SPL	Sound pressure level
VMS	Vessel Monitoring System

1 Introduction

Underwater sound maps are proposed as a tool to investigate the state of the underwater environment, see e.g. (Putland, de Jong, Binnerts, Farcas, & Merchant, 2022), (Sertlek, Slabbekoorn, Ten Cate, & Ainslie, 2019). These map the sound pressure field in the sea. Because most fishes and aquatic invertebrates are predominantly sensitive to particle motion , it is relevant to be able to quantify this aspect of the underwater sound field (Nedelec, Campbell, Radford, Simpson, & Merchant, 2016).

Sound particle motion and sound pressure are inseparable properties of the sound field. Guidelines for measuring sound particle motion are presented in (Nedelec, et al., 2021). Guidelines for modelling ocean ambient sound pressure have been published by the JOMOPANS project (de Jong C. , Binnerts, Robinson, & Wang, 2021). This report provides guidelines for modelling sound particle motion for producing sound particle motion maps.

Chapter 2 describes the relevant sound particle motion metrics and how these relate.
Chapter 3 describes the models that can be used for producing sound particle motion maps.
Chapter 4 describes how these models can be verified and validated.
Chapter 5 provides examples of calculated particle motion sound maps
Chapter 6 summarizes the guidelines for sound particle motion mapping.

Underwater acoustical terminology used in this report follows ISO 18405:2017, while vessel acoustical and bioacoustical terminology follow the SATURN terminology standard (Ainslie, et al., 2024).

2 Sound particle motion metrics

2.1 Sound pressure and particle motion

Sound is defined as "an alteration in pressure, stress or material displacement propagated via the action of elastic stresses in an elastic medium and that involves local compression and expansion of the medium, or the superposition of such propagated alterations" (International Organization for Standardization, 2017). Underwater (or water-borne) sound is often characterized in terms of its *sound pressure*, but the passage of sound causes motion of the medium in which it propagates. The motion of a *sound particle* (defined as the "smallest element of the medium that represents the medium's mean density") can be expressed in terms of its *sound particle displacement* (expressed in metres), *sound particle velocity* (expressed in metres per second) or *sound particle acceleration* (expressed in metres per second squared) or higher order derivatives (*jerk*, *snap*, etc.). These are all vector quantities, which can be expressed in Cartesian xyz-coordinates. By convention in underwater acoustics, the z axis is usually chosen to point vertically down from the sea surface, with x and y axes in the horizontal plane.

For small-amplitude sound waves in an otherwise stationary medium, the *sound particle velocity* $\boldsymbol{u}$ and *sound particle displacement* $\boldsymbol{\delta}$ are related by $\boldsymbol{u}(\boldsymbol{r},t) = \partial\boldsymbol{\delta}(\boldsymbol{r},t)/\partial t$ and the *sound particle acceleration* $\boldsymbol{a}$ and *sound particle velocity* $\boldsymbol{u}$ are related by $\boldsymbol{a}(\boldsymbol{r},t) = \partial\boldsymbol{u}(\boldsymbol{r},t)/\partial t$. The partial derivatives are evaluated at a fixed position (vector $\boldsymbol{r}$) and time (t). These formulae provide an approximation, with relative error of order $|u/c|$, where c is the speed of sound in the medium.

The sound particle displacement, velocity, and acceleration are all linked in the frequency domain by factors of $\omega = 2\pi\mathrm{i}f$. If one is known, the others are known. Therefore, it is useful to perform simulations in the frequency domain. The Fourier transforms of sound particle acceleration $\boldsymbol{A}$ and sound particle displacement $\boldsymbol{D}$ are related to the sound particle velocity via[1]:

$$\boldsymbol{A}(\boldsymbol{r},\omega) = \mathrm{i}\omega\boldsymbol{U}(\boldsymbol{r},\omega) \tag{1}$$

and

$$\boldsymbol{D}(\boldsymbol{r},\omega) = \boldsymbol{U}(\boldsymbol{r},\omega)/\mathrm{i}\omega \tag{2}$$

2.2 Sound particle motion levels

Sound particle displacement, velocity and acceleration are time-varying quantities. These can be quantified in terms of various statistical metrics. Procedures for selecting the appropriate metric(s) for characterizing the underwater sound to which animals are exposed, as a basis for assessing the potential effects of this sound exposure, are still in their infancy. The very limited and scattered set of available data on the wide variety of potential physiological and behavioural effects on very

[1] The sound field can be expressed in terms of its frequency (f) components via a Fourier transform:

$$p(r,t) = \int_{-\infty}^{\infty} P(r,f)\exp(+\mathrm{i}\omega t)\,\mathrm{d}f$$

$$u_r(r,t) = \int_{-\infty}^{\infty} U_r(r,f)\exp(+\mathrm{i}\omega t)\,\mathrm{d}f$$

where P is the *sound pressure spectrum* and U_r the *sound particle velocity spectrum* (ISO, 2017)

different species do not offer a clear case for a best choice from the various possible statistical metrics for quantifying the sound exposure in the context of potential impact assessment. In the current literature on impact of sound on aquatic wildlife, such as (Popper, et al., 2014) and (Southall, et al., 2019), there is a general agreement that the *mean-square* value (the integral over a specified time interval of the squared quantity, divided by the duration of the time interval) of sound pressure or sound particle displacement, velocity or acceleration is an appropriate metric for *continuous sound*. The square root of the mean-square value is known as the *root-mean-square*.

Short duration *impulsive sounds* are described in terms of *exposure* (the integral over a specified time interval of the squared quantity) and *peak* (e.g. the greatest magnitude of the quantity) metrics. Precise definitions of 'continuous' and 'impulsive' sounds are lacking, but ship sound is generally considered to be 'continuous' sound. Examples of sounds widely considered as 'impulsive' are the sounds generated by airguns for seismic surveys and the sounds generated by percussive pile driving.

For the sound particle motion mapping of shipping sound, we focus on mean-square metrics, comparable with the metrics used for sound pressure maps of shipping sound in, for example, the Jomopans project (de Jong C. , Binnerts, Robinson, & Wang, 2021).

The (International Organization for Standardization, 2017) standard defines the level of the mean-square sound particle displacement $\overline{\delta^2}$ as:

$$L_\delta = 10 \log_{10} \left(\frac{\overline{\delta^2}}{(1 \text{ pm})^2} \right) \text{ dB}, \tag{3}$$

the level of the (mean-square) sound particle velocity $\overline{u^2}$ as:

$$L_u = 10 \log_{10} \left(\frac{\overline{u^2}}{\left(1 \frac{\text{nm}}{\text{s}}\right)^2} \right) \text{ dB}, \tag{4}$$

and the level of the (mean-square) sound particle acceleration $\overline{a^2}$ as:

$$L_a = 10 \log_{10} \left(\frac{\overline{a^2}}{\left(1 \frac{\mu\text{m}}{\text{s}^2}\right)^2} \right) \text{dB}. \tag{5}$$

Noting that the sound particle displacement, velocity, and acceleration are three-dimensional vector quantities, the above definitions can be applied to each of the three vector-components as well as to the magnitude of the vectors, see below.

All three metrics require specification of the time interval over which the mean-square value is determined and of the frequency range:

Time interval

The mean-square value of continuous sound quantities is independent of the duration of the specified time interval (provided that that duration is selected within reasonable limits). For quantifying ship sound, the duration should be chosen sufficiently large to capture the time-varying properties of the sound generating mechanisms on the ship, such as the rotation period of the

propeller shaft and of the main rotating machinery. On the other hand, the duration should be limited to the period within which the movement of the ship(s) relative to the position where the sound is observed does not significantly affect the received sound.

Frequency range

Sound particle motion is primarily of interest for assessing the impact of sound exposure on fish and invertebrate species. (Hawkins, Johnson, & Popper, 2020) argue that the frequency range is a relevant attribute of sound exposure. (Popper, et al., 2014) summarize that hearing range and sensitivity varies considerably among fish species. Fish sense sound through vibration of the otolith organs in their inner ear, which means that they are primarily sensitive to particle motion. However, deformation of their swim bladder (or other internal gas volume) under influence of sound pressure contributes to the particle motion that reaches the inner ear, so that fish with swim bladders are also sensitive to sound pressure. The pressure sensitivity is higher when the gas volume is closer to the inner ear. In some fish species the gas volume is connected to the inner ear by a bony structure (the Weberian ossicles) resulting in an increase of the hearing sensitivity at higher frequencies. Some of these fishes are reported to respond to high intensity ultrasound (>10 kHz). Figure 2-1 (from (Popper, et al., 2014)) shows some published audiograms of particle motion-sensitive species. This illustrates that the lowest detectable level of sound particle acceleration increases significantly above 200 Hz for these examples. Assuming potential effects of particle motion on an aquatic animal are mainly limited to the animal's hearing range, although other species could potentially be sensitive to particle motion at other frequencies, this suggests that the frequency range for particle motion modelling can be tentatively limited to frequencies between 10 Hz and 1000 Hz (precautionarily selecting a somewhat broader frequency range than suggested by the audiograms in Figure 2-1).

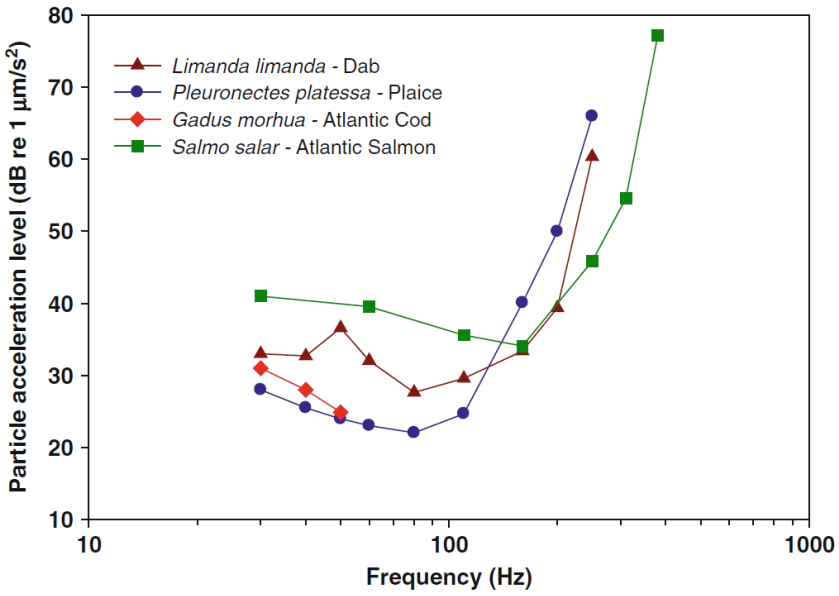

Figure 2-1 Examples of particle motion behavioural audiograms for four fish species: Atlantic salmon (Salmo salar; (Hawkins & Johnstone, 1978)); plaice (Pleuronectes platessa; (Chapman & Sand, 1974)); dab (Limanda limanda; (Chapman & Sand, 1974)); and Atlantic cod (Gadus morhua; (Chapman & Hawkins, 1973)). Source: Fig.3.1 from (Popper, et al., 2014).

The standard definitions of sound particle velocity level and sound particle acceleration level (ISO, 2017) are in terms of the mean-square value of the magnitude of the corresponding vectors, over a specified time interval, see also (Nedelec, et al., 2021). In this study we propose adding similar definitions for the magnitude of individual components of the vector. These are spelled out below for metrics related to sound particle acceleration. These definitions apply in a polar co-ordinate system with the sound source at the central vertical axis. The azimuthal coordinate of the sound particle acceleration vector is ignored here, because that will be zero in an axisymmetric environment.

- **Mean-square radial sound particle acceleration** = integral over a specified time interval of square of the magnitude of the **radial component** of sound particle acceleration, divided by the duration of the time interval, for a specified frequency range (symbol $\overline{a_r^2}$).
- **Mean-square vertical sound particle acceleration** = integral over a specified time interval of square of the magnitude of the **vertical component** of sound particle acceleration, divided by the duration of the time interval, for a specified frequency range (symbol $\overline{a_z^2}$)
- **Time-integrated squared radial sound particle acceleration** = integral of the square of the magnitude of the **radial component** of sound particle acceleration, for a specified frequency range (symbol E_{a_r})
- **Time-integrated squared vertical sound particle acceleration** = integral of the square of the magnitude of the **vertical component** of sound particle acceleration, for a specified frequency range (symbol E_{a_z})

The levels associated with these quantities are defined as:

- **Mean-square radial sound particle acceleration level** = ten times the logarithm to the base 10 of the ratio of the *mean-square radial sound particle acceleration* to the specified reference value a_0^2, multiplied by 1 decibel (abbreviation: PALr; symbol L_{a_r})
- **Mean-square vertical sound particle acceleration level** = ten times the logarithm to the base 10 of the ratio of the *mean-square vertical sound particle acceleration* to the specified reference value a_0^2, multiplied by 1 decibel (abbreviation: PALz; symbol L_{a_z})
- **Time-integrated squared radial sound particle acceleration level** = ten times the logarithm to the base 10 of the ratio of the *time-integrated squared radial sound particle acceleration* to the specified reference value $E_{a,0}$, multiplied by 1 decibel (abbreviation: PAELr; symbol L_{E,a_r})
- **Time-integrated squared vertical sound particle acceleration level** = ten times the logarithm to the base 10 of the ratio of the *time-integrated squared vertical sound particle acceleration* to the specified reference value $E_{a,0}$, multiplied by 1 decibel (abbreviation: PAELz; symbol L_{E,a_z})

The reference value of mean-square sound particle acceleration, a_0^2, is 1 (µm/s²)².
The reference value of time-integrated squared sound particle acceleration, $E_{a,0}$, is 1 (µm/s²)² s.

Similar metrics can be defined for sound particle velocity, noting that;
The reference value of mean-square sound particle velocity, u_0^2, is 1 (nm/s)².
The reference value of time-integrated squared sound particle velocity, $E_{u,0}$, is 1 (nm/s)² s.

2.3 Sound intensity

The time-averaged sound intensity is defined as the integral over a specified time interval of the product of sound pressure and the sound particle velocity vector, divided by the duration of the time interval, for a specified frequency range (International Organization for Standardization, 2017): $\boldsymbol{I}(t) = \frac{1}{T}\int_0^T p(t)\boldsymbol{u}(t)\mathrm{d}t$. Thus, sound intensity is a vector that quantifies the sound power propagating per unit area, including the direction of that propagation. Intensity can be mapped including direction in a so-called 'quiver plot', displaying vectors as arrows.

In the frequency domain, the active sound intensity is:

$$\boldsymbol{I}(\omega) = \frac{1}{2}\mathrm{Re}\{P(\omega)\boldsymbol{U}^*(\omega)\} \tag{6}$$

with P the Fourier transform of the sound pressure, $\boldsymbol{U}$ the Fourier transform of the sound particle velocity vector, and $\boldsymbol{U}^*$ the complex conjugate of $\boldsymbol{U}$.

2.4 Sound power

The sound power radiated by the sound source is partly transmitted into the seabed and partly stays in the fluid waveguide. At horizontal range r, the radial power in the axisymmetric fluid waveguide (W_{water}) can be obtained by integrating the radial intensity $I_r(r,z)$, over the vertical coordinate z from $z = 0$ at the water surface to $z = H$ at the seabed:

$$W_{\mathrm{water}}(r) = 2\pi r \int_0^{H(r)} I_r(r,z)\mathrm{d}z, \tag{7}$$

The power transmitted into the seabed up to that range follows from the integral of the component of the intensity $I_n\big(r,H(r)\big)$ that is locally normal to the seabed:

$$W_{\mathrm{seabed}}(r) = 2\pi \int_0^r I_n(r,H(r))\, r \sqrt{1+\left(\frac{\mathrm{d}H(r)}{\mathrm{d}r}\right)^2}\ \mathrm{d}r, \tag{8}$$

The square root term in this equation accounts for the surface area of a locally sloping seabed for each horizontal step $\mathrm{d}r$.

In cases where the absorption in water can be ignored, the total power is invariant with range:

$$W_{\mathrm{water}}(r) + W_{\mathrm{seabed}}(r) = W_{\mathrm{tot}}. \tag{9}$$

Hence, calculation of the power transmitted in the water and into seabed as function of range can be used to check if the numerical implementation of the propagation model for sound pressure and sound particle motion is correct.

2.5 Propagation loss

Sound pressure propagation loss is defined by ISO 18405 (ISO, 2017) and can be calculated from:

$$N_{\mathrm{PL},p} \equiv L_{\mathrm{S}} - L_p, \tag{10}$$

with L_p the sound pressure level, expressed in dB re 1 µPa², L_S the source level, in dB re 1 $(\mu\mathrm{Pa\ m})^2$, and $N_{\mathrm{PL},p}$ the propagation loss in dB re 1 m².

Sound particle velocity propagation loss $N_{\mathrm{PL},u}$ is defined by SATURN (Ainslie, et al., 2024) and can be calculated from:

$$N_{\mathrm{PL},u} \equiv L_{\mathrm{S}} - L_u, \tag{11}$$

with L_u the sound particle velocity level, in dB re 1 $(\mathrm{nm/s})^2$, and $N_{\mathrm{PL},u}$ expressed in dB re 1 $\left(\frac{\mu\mathrm{Pa\ m}}{\mathrm{nm/s}}\right)^2$.

Sound particle acceleration propagation loss $N_{\mathrm{PL},a}$ can be defined by SATURN as:

$$N_{\mathrm{PL},a} \equiv L_{\mathrm{S}} - L_a, \tag{12}$$

with L_a the sound particle acceleration level, in dB re 1 $(\mu\mathrm{m/s^2})^2$, and $N_{\mathrm{PL},a}$ expressed in dB re 1 $\left(\frac{\mu\mathrm{Pa\ m}}{\mu\mathrm{m/s^2}}\right)^2$.

By analogy, propagation loss can also be calculated for individual vector components, e.g.:

Radial sound particle acceleration propagation loss N_{PL,a_r}:

$$N_{\mathrm{PL},a_r} \equiv L_{\mathrm{S}} - L_{a_r}, \tag{13}$$

Vertical sound particle acceleration propagation loss N_{PL,a_z}:

$$N_{\mathrm{PL},a_z} \equiv L_{\mathrm{S}} - L_{a_z}, \tag{14}$$

2.6 Scaled impedance

In the idealized case of an acoustic plane wave propagating in a lossless free-field environment, sound particle velocity u and sound pressure p are directly related via the characteristic specific acoustic impedance of sea water $z_w = \rho_w c_w$ of the medium in which the wave is propagating: $p = z_w u$, where ρ_w is the volumetric density of the medium and c_w the speed of sound.

In specific situations, as discussed in the following subsections, close to sound sources and in confined environments, such as in shallow water and in laboratory tanks, the ratio of sound particle velocity and sound pressure can deviate significantly from this simple proportionality. The **scaled impedance** has been proposed by (Jansen, Prior, & Brouns, 2019) to quantify this deviation:

$$\zeta_{\mathrm{sc}} = \frac{p}{z_w |u|} \tag{15}$$

Here $|u| = \sqrt{u_x^2 + u_y^2 + u_z^2}$ is the magnitude of the particle velocity vector.

In the frequency domain ($\omega = 2\pi f$), the Fourier transform of the scaled impedance is:

$$Z_{\mathrm{sc}}(\omega) = \frac{P(\omega)}{z_w |U(\omega)|} \tag{16}$$

with P the Fourier transform of the sound pressure and U the Fourier transform of the magnitude of the sound particle velocity.

Typically, the scaled impedance deviates from 1 in the sound field in bounded environments, such as laboratory tanks and aquaria, and at distances within about one acoustic wavelength from sources and discontinuities such as the seas surface and the sea bed in shallow water. This is illustrated in the following examples.

2.6.1 Close to acoustic point source

One example of a situation where the scaled impedance deviates from 1 is the nearfield of an acoustic point source in a lossless free-field environment. Based on the definition of acoustic far field in ISO 18405 (ISO, 2017), the distance from the source that is smaller than π times the square of the largest dimension of the source divided by the acoustic wavelength can be identified as the nearfield region. Outside this region, in the far field, sound particle velocity and sound pressure are in phase and vary inversely with distance. At frequencies where the radius a of a monopole sound source is small compared to the acoustic wavelength ($k_0 a \ll 1$), the radial particle velocity close to the source decays with range r according to $U_r = \frac{P}{z_w}\left(1 - \frac{\mathrm{i}}{k_w r}\right)$, see e.g. (Gray, Rogers, & Zeddies, 2016), so that

$$Z_{\mathrm{sc}} = \left(1 - \frac{1}{k_w^2 r^2}\right)^{-1/2} \tag{17}$$

Hence $(Z_{\mathrm{sc}} - 1) \leq 0.01$ for $k_w r \geq 7$. So, the scaled impedance deviates less than 1% from $Z_{\mathrm{sc}} = 1$ at distances r larger than about one acoustic wavelength from the source.

2.6.2 Close to seabed and sea surface

The sea surface acts as a pressure release boundary ($P \approx 0$) at which the scaled-impedance is zero as well ($Z_{\mathrm{sc}} \approx 0$). The boundary condition at the seabed depends on the geoacoustic properties of the seabed. If the seabed is much harder than water (the characteristic impedance much higher), the scaled impedance at the seabed becomes very large ($Z_{\mathrm{sc}} \to \infty$). These effects are typically less relevant at distances greater than a quarter wavelength from sea surface and seabed (see §4.1 and Annex B).

2.6.3 In a shallow water waveguide below cut-off

The good practice guide (Nedelec, et al., 2021) recommends that “particle motion should be measured when below the cut-off frequency of the waveguide”, because it then cannot be calculated from a pressure measurement. Below the cut-off frequency, sound waves will not propagate to long distances along a shallow-water waveguide formed by the bottom and the surface (or the tank walls if in a tank). Consequently, the scaled impedance will deviate from 1 in this condition.

The cut-off frequency f_c for a shallow-water wave guide of depth H with uniform sound speed c_w in the water and uniform compressional wave speed c_s in the seabed can be estimated as (Jensen, Kuperman, Porter, Schmidt, & Tolstoy, 2011):

$$f_c \approx \frac{c_w}{4H\sqrt{1-(c_w/c_s)^2}}. \quad (18)$$

2.6.4 Close to a seabed supporting subsonic boundary waves

(Gray, Rogers, & Zeddies, 2016) provide another example, of the sound field close to a seabed, if the wave propagation speed along the seabed c_x is slow compared to the speed of sound in water: $c_x \ll c_0$. This situation can occur when the seabed supports shear and (Scholte) interface waves. In that case, the wavenumber component perpendicular to the boundary is imaginary $k_z = \sqrt{k_0^2 - k_x^2} \approx ik_x$ so that the sound field decays exponentially with increasing distance from the seabed: $P(x,z) \approx P_0(x)e^{-k_x z}$, $U_x(x,z) = \frac{P(x,z)}{z_w}\left(\frac{k_x}{k_0}\right)$ and $U_z(x,z) = \frac{P(x,z)}{z_w}\left(\frac{ik_x}{k_w}\right)$. The 90° phase difference between U_x and U_z corresponds with a characteristic circular pattern of surface waves. The scaled impedance of these waves is:

$$Z_{sc} \approx \frac{1}{\sqrt{2}}\left(\frac{k_x}{k_w}\right) = \frac{1}{\sqrt{2}}\left(\frac{c_w}{c_x}\right) \gg 1. \quad (19)$$

Due to the exponential decay, the particle motion amplitude decays to less than 0.2 % of the amplitude at the seabed at distances r larger than about one wavelength (λ_x) from the surface.

3 Calculating sound particle motion maps

There are multiple metrics of particle motion that can be represented in sound maps. For selecting the appropriate metrics, one needs to consider that the sound field has more components than can be represented on a two-dimensional spatial map.

For the purpose of the SATURN project, the focus is on producing statistical sound maps of the underwater sound from shipping, that can be used as input for assessment of the environmental status of sea areas (such as for the EU Marine Strategy Framework Directive) and for marine spatial planning. Consequently, detailed calculations of the sound particle motion field close to sources or to the seabed and in shallow water (<10 m deep) close to the shore is not considered.

3.1 Considerations for producing sound maps

Many choices have to be made to make sound maps. These choices must be specified with the sound maps to enable a proper interpretation. Here are examples of the various choices that were made for the Jomopans North Sea sound maps (de Jong C. , Binnerts, Robinson, & Wang, 2021). The Jomopans maps were used in SATURN to estimate corresponding sound particle acceleration level maps (see Chapter 5).

Metrics

The Jomopans sound maps represent sound pressure level due to the underwater radiated sound from ships and wind. Sound maps were also provided for alternative metrics such as 'excess level' and 'dominance'.

In SATURN, the modelling capability has been extended to calculate maps that represent sound particle motion, here illustrated in maps of the sound particle acceleration level (based on the magnitude of the sound particle acceleration vector), see chapter 5.

Temporal statistics

The Jomopans sound maps presented percentiles (50% and 90%) of the sound pressure level (SPL) distribution measured over one-month and one-year periods. The statistic was based on calculated steady state SPL maps in 10 minute time steps. Here, 'steady state' implies that the temporal observation window is long enough for the SPL to be independent of the duration of the window, and short enough to assume that at each time step all sources are stationary at their actual positions, while their steady state source level remains determined by the actual source parameters (such as vessel speed).

Frequency

Broadband values of the SPL metrics are calculated, including the full frequency range covered by the decidecade bands with centre frequencies from 10 Hz up to 20 kHz, or the decade bands covered by the decidecade bands with nominal centre frequencies from 20 Hz to 160 Hz, 200 Hz to 1.6 kHz and 2 kHz to 20 kHz respectively. Propagation loss is calculated at the centre frequencies of the decidecade bands only, as proxy for the broadband propagation loss in the decidecade.

Spatial statistics

Sound maps represent a depth-averaged value of the metrics at the centroid of each grid cell, without spatial averaging. The grid for the Jomopans sound maps has a resolution of 0.05 degrees longitude and 0.025 degrees latitude (about 3 km × 3 km in the North Sea). The depth average is here calculated over 10 equally spaced receiver points between 1 m below the water surface and 1 m above the seabed.

Spatial processing

In order to reduce the computational complexity of the modelling, sound maps are generally obtained using an "$N \times 2\mathrm{D}$ approach", implying that the modelling results are obtained by means of two-dimensional linear interpolation of the depth averaged values between radial transects (slices/radials) from each source. The selected number of radial transects, their length and the spatial resolution along the transects can all have an effect on the results and hence need to be specified. The Jomopans sound maps were made based calculations along 16 radial transects per source, with a horizontal resolution of 100 m, from a location at 100 m from the source location to a maximum distance of 400 km, or to the location where the water depth was less than 5 m. The bathymetry along the transects was linearly interpolated from the EMODnet[2] 0.125 minute × 0.125 minute grid. The computation time was reduced significantly by means of source gridding. This enabled repeated use of stored data (look-up table) from a single calculation of propagation loss between predefined source and receiver grids for shipping sound map calculations over multiple time steps. For the Jomopans North Sea sound maps the source grid was based on the receiver grid, shifted by one half of the grid resolution and slightly refined by adding intermediate source grid positions at 0.025° latitude resolution, while avoiding overlap with the receiver grid points.

3.2 Selection of models

3.2.1 Ship source level model

Ship traffic at sea is monitored by AIS (Automatic Identification System) and VMS (Vessel Monitoring System) services. Recordings from these systems are used to provide the input for calculating ship sound maps. Because these systems were not specially designed for this purpose, the recorded data needs to be processed. This processing includes checks of validity and consistency and interpolation of the individual ship trajectories to the regular temporal grid for the sound maps.

The Jomopans-ECHO model (MacGillivray & de Jong, 2021) was used for the Jomopans maps. It provides an estimated statistical ship source level spectrum based on the ship speed over ground, ship length and ship type parameters from the AIS data, for a nominal source depth of 6 m below the water surface, with a statistical uncertainty of about 6 dB.

3.2.2 Ship sound propagation models

There are many underwater acoustical models that compute the propagation of a sound at a specific frequency, see (de Jong C. , Binnerts, Robinson, & Wang, 2021) for an overview.

[2] https://www.emodnet-bathymetry.eu/

In SATURN task T2.3 the focus was on the following modelling approaches, that allow calculating sound particle motion:

1 Wavenumber integration method
   - Calculates a numerical solution to the spectral (wavenumber) integral of solutions to the depth-separated wave equation (Jensen, Kuperman, Porter, Schmidt, & Tolstoy, 2011) in range-independent environments. The OASES code[3] include the option to calculate the sound particle velocity vector at specified locations.

2 Parabolic equation (PE) method
   - Separates the wave equation into incoming and outgoing solutions and then calculates the acoustic field, neglecting incoming waves (back-scattered energy) using a marching algorithm. The mostly used class of available PE models for underwater sound employs the split-step Padé expansion solution (Collins, 1993). Standard PE implementations do not provide a direct output in terms of particle motion vectors, but these can be obtained by calculating the spatial derivatives of the sound pressure field, see Annex A.

3 Finite element (FE) method
   - Grids the calculation environment at sub-wavelength spacing and then solves the wave equation in space and time or frequency, see e.g. (Murphey & Chin-Bing, 1989). FE models can relatively easily take into account range dependence and shear properties of seabed materials. Particle acceleration components are directly calculated by most FE model implementations.

4 Image source (IS) method
   - Sums the analytical Green's functions for a series of image sources that represent reflections at water surface and seabed in a range-independent Pekeris waveguide (Pekeris, 1948). In the frequency domain, the sound particle velocity spectrum can be calculated analytically from the Green's function (Pierce, 2019).

The Jomopans sound pressure level maps for ships and wind on the North Sea were calculated using TNO's Aquarius 3 model, which combines a range-dependent adiabatic normal mode sum for the lower frequency bands with a flux integral model for the higher frequency bands (Sertlek, Ainslie, & Heaney, 2018). This model was verified against other models for the benchmark tests, see (de Jong C. , Binnerts, Robinson, & Wang, 2021).

The Aquarius 3 model does not calculate the sound particle motion components of the sound field. The corresponding sound particle acceleration level maps were estimated based on scaling, see Chapter 5.

3.2.3 Wind source and sound propagation models

Wind noise can be calculated with the wind noise source and propagation models based on the semi-empirical expressions described in chapter 8 of in (Ainslie M. , Principles of Sonar Performance Modeling, 2010). The method used by the model is described by (Ainslie, Harrison, &

[3] https://acoustics.mit.edu/faculty/henrik/oases.html

Zampolli, 2011). This model was applied for the Jomopans wind noise maps (de Jong C. , Binnerts, Robinson, & Wang, 2021), (de Jong C. , Binnerts, de Krom, & Gaida, 2022).

The wind noise model does not directly calculate the sound particle motion components of the sound field. Extending this model has not been further investigated in SATURN.

3.3 Scaling from sound pressure level maps

Analysis of the acoustic impedance for benchmark scenarios (Oppeneer, de Jong, Binnerts, Wood, & Ainslie, 2023) confirmed that the magnitude of the sound particle velocity vector can be directly estimated from the sound pressure field in shallow water scenarios, except at distances within one wavelength of the source, or within a distance of a few water depths from the source at frequencies where the wavelength exceeds the water depth. This allows for a straightforward estimation of sound particle motion sound maps from SPL sound maps, see §4.1.1.

A broadband (BB) sound particle velocity level **(PVL) map** can be calculated by scaling the SPL map with the characteristic specific impedance of the fluid (ρc):

$$L_{u,\mathrm{BB}} = L_{p,\mathrm{BB}} - 10\log_{10}\left((\rho c)^2 \frac{(1\ \mathrm{nm/s})^2}{(1\ \mu\mathrm{Pa})^2}\right)\ \mathrm{dB} \approx L_{p,\mathrm{BB}} - 63.5\ \mathrm{dB} \tag{20}$$

A broadband sound particle acceleration level **(PAL) map** can be calculated from the spectral PVL map:

$$L_{a,\mathrm{BB}} = 10\log_{10}\left(\sum_{n=10}^{n=43}\left(10^{\frac{L_u(f_n)}{10\ \mathrm{dB}}}(2\pi f_n)^2 \frac{(1\ \mathrm{nm/s})^2}{(1\ \mu\mathrm{m/s^2})^2}\right)\right)\ \mathrm{dB} \tag{21}$$

for decidecade centre frequencies $f_n = 10^{n/10}$ Hz.

This approach has been chosen to calculate example sound particle acceleration level maps for the North Sea (see Chapter 5).

4 Model verification and validation

Different existing models for underwater sound propagation have the potential to calculate sound particle motion (displacement, velocity or acceleration) in addition to sound pressure.

The quality of the applied model needs to be tested and demonstrated. The ISO/IEC Systems and software Quality Requirements and Evaluation (SQuaRE) family of standards provides guidelines for the development of measures for evaluating the quality of systems and software to meet the specified requirements, and provides a common language for describing quality characteristics. Standard (ISO/IEC 25002, 2024) defines:

- **Verification:** confirmation, through the provision of objective evidence, that specified requirements have been fulfilled.
- **Validation:** confirmation, through the provision of objective evidence, that the requirements for a specific intended use or application have been fulfilled

The Jomopans terminology standard (Robinson & Wang, 2021) explains that model **verification** is a demonstration that the model correctly calculates the outputs for specified inputs. Model **validation** also demonstrates that the model outputs reflect an adequate representation of physical reality. Validation requires comparison to physical measurements, or to exact analytic solutions that are regarded as a good representation of the underlying physics. Model **benchmarking** is presented as a useful tool that sits between verification and validation. Good agreement between the outputs of different models for a series of well-defined scenarios provides confidence in the individual models, and is a strong indicator of likely validation, especially if the different models adopt different modelling approaches.

4.1 Model benchmark scenarios

To support a reliable implementation of shallow water sound propagation models, SATURN presents model benchmark solutions for three shallow-water scenarios. Shallow water here refers to water depths less than 200 m in which sound propagation is affected by interaction of the sound with sea surface and seabed. The scenarios include a step-by-step increase of complexity, from a fluid to a solid sediment (adding shear properties) and from range-independent to range-dependent (adding horizontal variation in water depth).

The model benchmark study was published in (Oppeneer, de Jong, Binnerts, Wood, & Ainslie, 2023) Input data and selected model solutions for the scenarios are summarized in Annex B. Solutions are calculated at three frequencies (25, 100 and 400 Hz).

Four different types of models were tested: a finite element (FE) model, a parabolic equation (PE) model, a wavenumber integration (WI) model, and an image source (IS) model. All models produced very similar results of the depth-averaged sound pressure and sound particle velocity propagation loss for the scenarios in which they can be applied. Close to the source, at ranges smaller than a few water depths, PE and WI solutions deviate from the FE and IS solutions, which are considered more applicable at short range. At larger ranges, the IS solutions at the lowest frequencies (25 and 100 Hz) deviate from the others, because the approximations in that approach limit the applicability to higher frequencies.

Since the FE model does not simplify the wave equation, it is assumed to be the most accurate method for generating a solution for both pressure and particle motion. The FE model implementation was verified by reproducing the results from (Collins & Evans, 1992) for the ASA penetrable wedge scenario (benchmark scenario III).

4.1.1 Prediction of sound particle velocity from sound pressure

In many situations (see section 2.6) the scaled impedance is close to one, so that the sound particle velocity can be estimated from scaling the sound pressure with the characteristic specific impedance of water, particularly if one is not interested in detailed results at single locations and single frequencies. To illustrate this, Figure 4-1 shows the scaled impedance calculated by the FE model for the three benchmark scenarios. These show the expected reduction of the scaled impedance within about one quarter of a wavelength below the sea surface (i.e. 15 m at 25 Hz, 4 m at 100 Hz and 1 m at 400 Hz). In the rest of the fluid domain, The scaled impedance deviates locally from 1 (i.e. $20\log_{10}(Z_{sc}) = 0$ dB), but the locations vary strongly with frequency so that the deviations will be less relevant when considering frequency bands. Also near the seabed the scaled impedance is close to 1 for these scenarios.

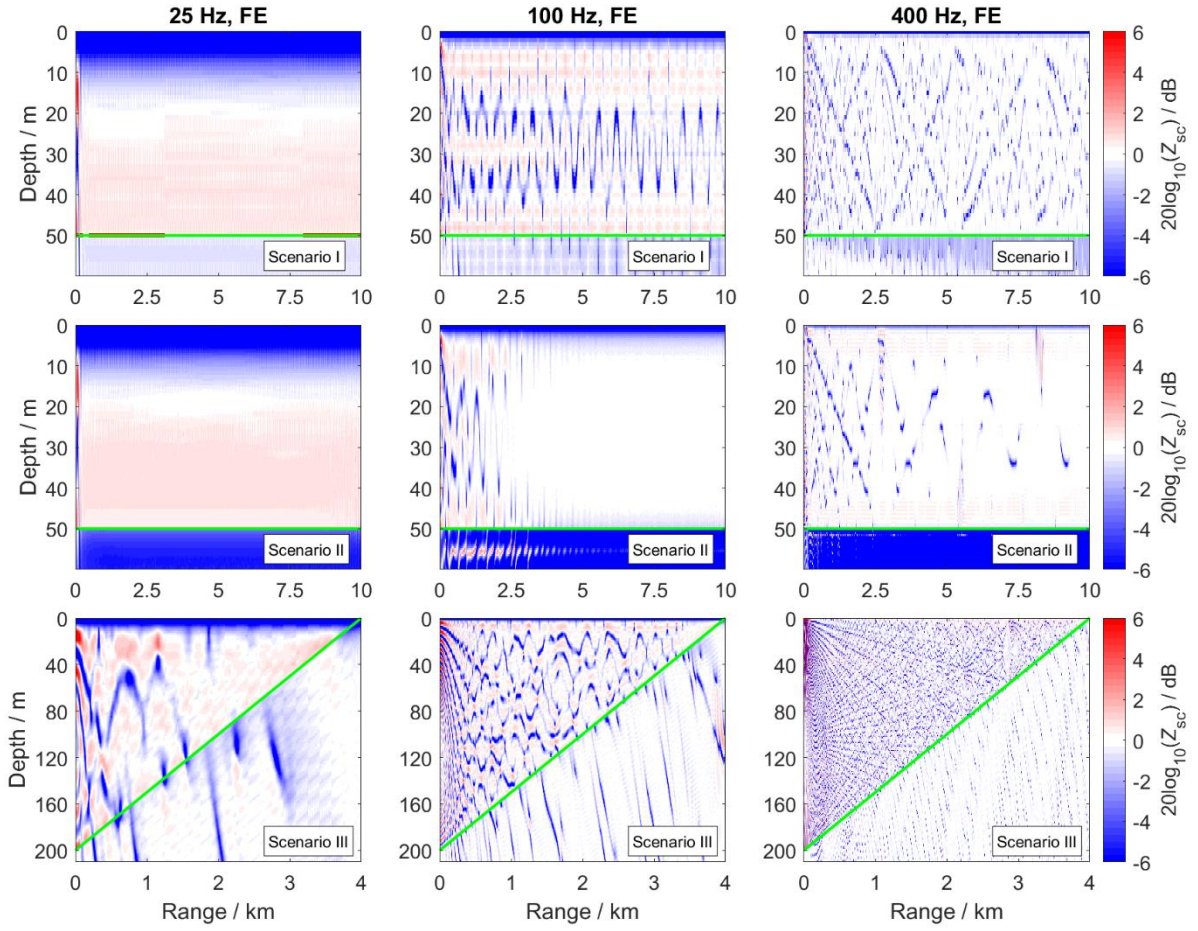

Figure 4-1 Scaled impedance), results from FE calculations for the three scenarios and frequencies. The green line indicates the location of the seabed.

Figure 4-2 presents the error in the estimation of depth averaged sound particle velocity from depth averaged sound pressure for the three scenarios and three frequencies, for the results of the FE model. This error is calculated as:

$$\mathrm{DA}\left(N_{\mathrm{PL},u}\right) - \mathrm{DA}\left(N_{\mathrm{PL},p}\right) + 63.5\ \mathrm{dB} \tag{22}$$

At horizontal ranges beyond about 20 m (less than one water depth) from the source the error is less than 1 dB for the magnitude of the sound particle velocity. At ranges beyond 200 m, where the radial component of the sound particle velocity dominates the magnitude, the error is less than 1 dB for the radial component as well.

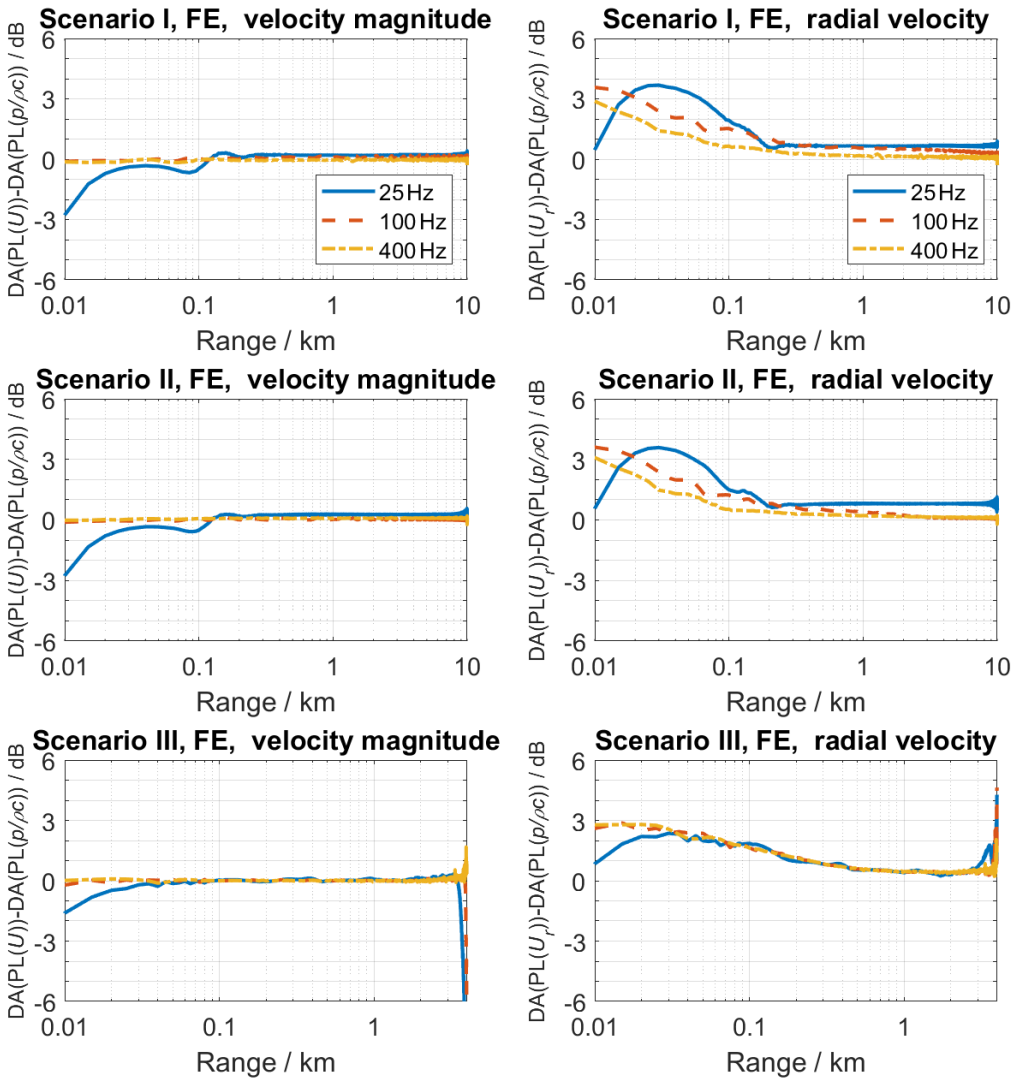

Figure 4-2 Difference between depth-averaged sound particle velocity propagation loss (left: $DA(N_{PL,u})$ and right $DA(N_{PL,u_r})$ in dB re 1 $\left(\frac{\mu Pa\ m}{nm/s}\right)^2$) and a prediction of sound particle velocity loss from depth averaged sound pressure propagation loss ($DA(N_{PL,p})$ in dB re 1 m^2), for the results from FE calculations for the three scenarios and frequencies

4.1.2 Power flow

Figure 4-3 shows the sound power flow (eqs.7-9) into fluid waveguide and seabed as a function of range, from FE calculations for the three benchmark scenarios (Annex B) at the three selected frequencies. This confirms that the total power flow does not vary strongly with range, which is a good check of the correct implementation of the models.

At short ranges (up to about 100 m), the power flows mainly in the water. At larger ranges, the power flow in the water waveguide decays with range, due to sound power transmission into the seabed. Shear waves in the sediment increase this decay. In the deeper range-dependent Scenario III, the power flow into the sediment is less prominent.

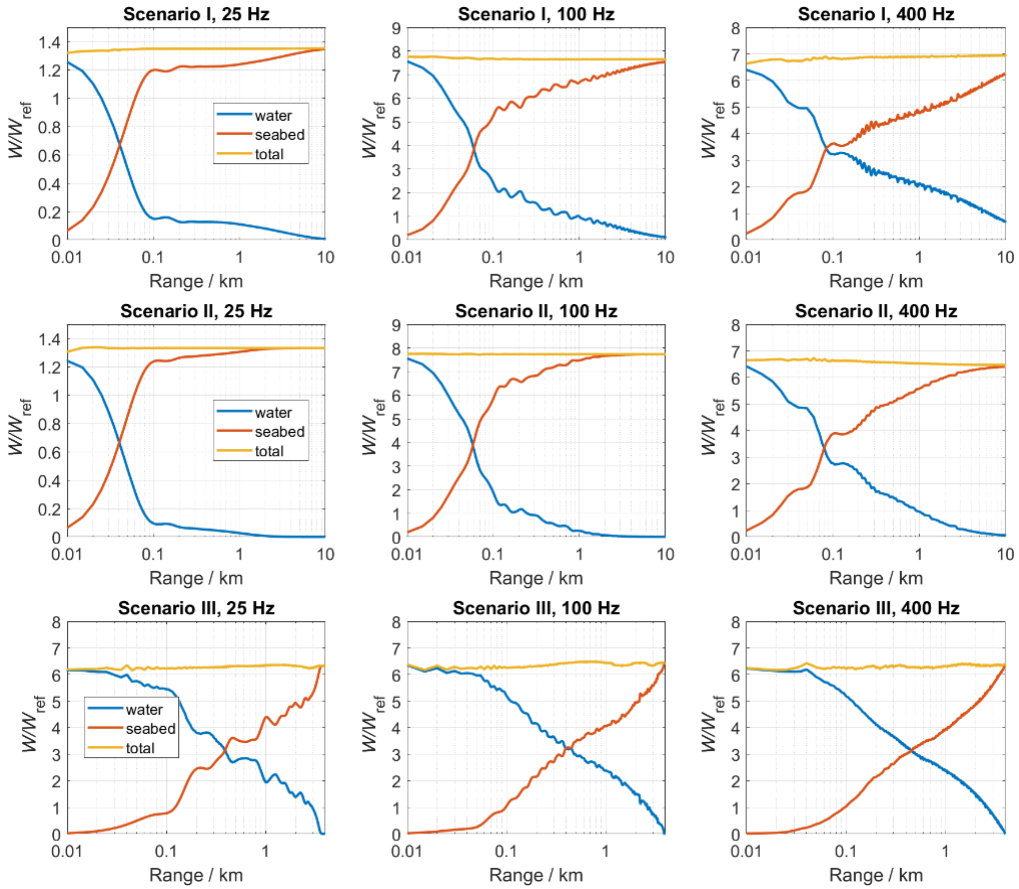

Figure 4-3 Sound power flow in the water (W_{water}), and into the seabed (W_{seabed}), calculated using equations (7) and (8), and the total sound power flow (W_{source}) radiated from the source to a distance r, from the FE calculations for the three scenarios and frequencies. The power is scaled by $W_{ref} = F/Z_0$, with F the source factor and Z_0 the characteristic specific impedance of water.

4.2 Model validation

The current best-practice for measuring sound particle motion has been summarized in a guidance document (Nedelec, et al., 2021), but there are very little data available that are suited for validating sound particle motions.

For model validation, a coherent set of data must be collected that consist of:

- Vector sensor data (three-dimensional sound particle accelerations)
- Detailed information about the used vector sensor: type, frequency range, sensitivity, calibration, noise floor, dynamic range, mounting configuration, three-dimensional location
- Hydrophone data (sound pressure, preferably collocated with the vector sensor)
- Detailed information about the used hydrophone: type, frequency range, sensitivity, calibration, noise floor, dynamic range, mounting configuration, three-dimensional location
- Environmental data: water depth, sound speed profile, sediment sound speed, density and absorption, wind speed
- Source data: three-dimensional location and source level of the sound source(s).

Because none of the datasets that could be made available to the SATURN project appeared to be complete, it was decided to perform a dedicated measurement trial. This trial and the analysis of the results are presented as an example of a model validation study in Annex C.

TNO deployed its particle motion measurement rig at a location in the North Sea, in the The Hague offshore test area[4]. The rig was deployed from a rigid-hull inflatable boat (RHIB) on the seabed at about 15 depth. It collected data from the sound produced by a small controlled airgun source during various runs with the RHIB at different distances from the rig.

Comparison between the measured and modelled propagation loss shows that the average model-data differences for PL and PVPLr are generally within ±6 dB for the frequency bands from 100 Hz to 1 kHz. The measured PL is generally substantially higher than modelled below 100 Hz. The measured PVPLz is 20 to 40 dB higher than the modelled PVPLz.

Differences are cause by uncertainties in modelling and measurements. The large discrepancy in PVPLz is mainly due to uncertainty in the orientation of the vector sensor, because the compass logger (orientation sensor) failed. One obvious cause for model-data differences in PL and PVPL is the uncertainty in the geo-acoustic modelling, as illustrated by varying the assumed sediment properties in the model calculations (Annex C). This was also identified as one of the main causes of uncertainty in the Jomopans shipping noise maps (Putland, de Jong, Binnerts, Farcas, & Merchant, 2022).

[4] https://proeftuinopdenoordzee.nl/

5 Sound map examples

The scaled impedance relates the sound pressure and sound particle velocity fields. It was calculated for the three benchmark scenarios (§4.1) to determine if there are regions where particle motion modelling is considered necessary and where a simple free field solution can yield a good approximation. It was shown that the scaled impedance field in these scenarios is very close to unity at most locations in the water waveguide (Oppeneer, de Jong, Binnerts, Wood, & Ainslie, 2023). Deviations from a value of unity mainly occur within about a quarter wavelength from the air-water interface and the seabed, and within a distance of about one wavelength from the source (§2.6.1), extending to about 3 water depths if the water depth is smaller than the wavelength. Outside these regions, the sound particle velocity field in a shallow water waveguide can be reasonably well estimated by dividing the sound pressure by the characteristic specific impedance of the fluid. This applies in particular for the depth-averaged North Sea sound maps (de Jong C. , Binnerts, Robinson, & Wang, 2021), see section 5.1.

5.1 North Sea sound maps (shipping and wind)

Figure 5-1 shows sound maps representing the annual median sound pressure level (SPL), sound particle velocity level (PVL) and sound particle acceleration level (PAL) from shipping and wind on the North Sea in 2020. Based on the suggestion that the frequency range for particle motion modelling can be tentatively limited to frequencies between 10 Hz and 1000 Hz (§2.2) these maps are made for a two-decade frequency bandwidth (8.91 Hz to 891 Hz)[5], including the decidecade bands with nominal centre frequencies 10 Hz to 800 Hz.

The **SPL map** was calculated in the Jomopans project (de Jong C. , Binnerts, de Krom, & Gaida, 2022).

The **PVL map** is calculated by scaling the SPL maps with the characteristic specific impedance of the fluid (eq.(20)). and the **PAL map** calculated from the spectral PVL map (eq.(21)).

Because the colour range for the PVL map is scaled to that of the SPL maps, according to eq.(20), the SPL and PVL maps look equal. The PAL map shows that the highest broadband PAL values are more focussed around shipping routes than the corresponding SPL and PVL values. This is because the main energy in the PAL spectra occurs at higher frequencies than in the SPL and PVL spectra, as illustrated by the spectra shown in Figure 5-2. The propagation loss is higher at higher frequencies, so that PAL decays faster with increasing distance from the shipping routes than SPL and PVL. Figure 5-2 (d) illustrates that the broadband SAL strongly depends on the selected upper limit of the frequency range (here extended to 22.4 kHz). This choice depends on the frequency range of interest for the application of the maps and must be guided by information on the frequency sensitivity of the considered species.

The values in the PVL and PAL maps can be directly compared to dose-effect relationships that indicate, for example, the risk of an effect on aquatic animals that are sensitive to particle motion, once these become available.

[5] This two-decade frequency band is named ‘band BC’ by the ADEON project (Ainslie, et al., 2018).

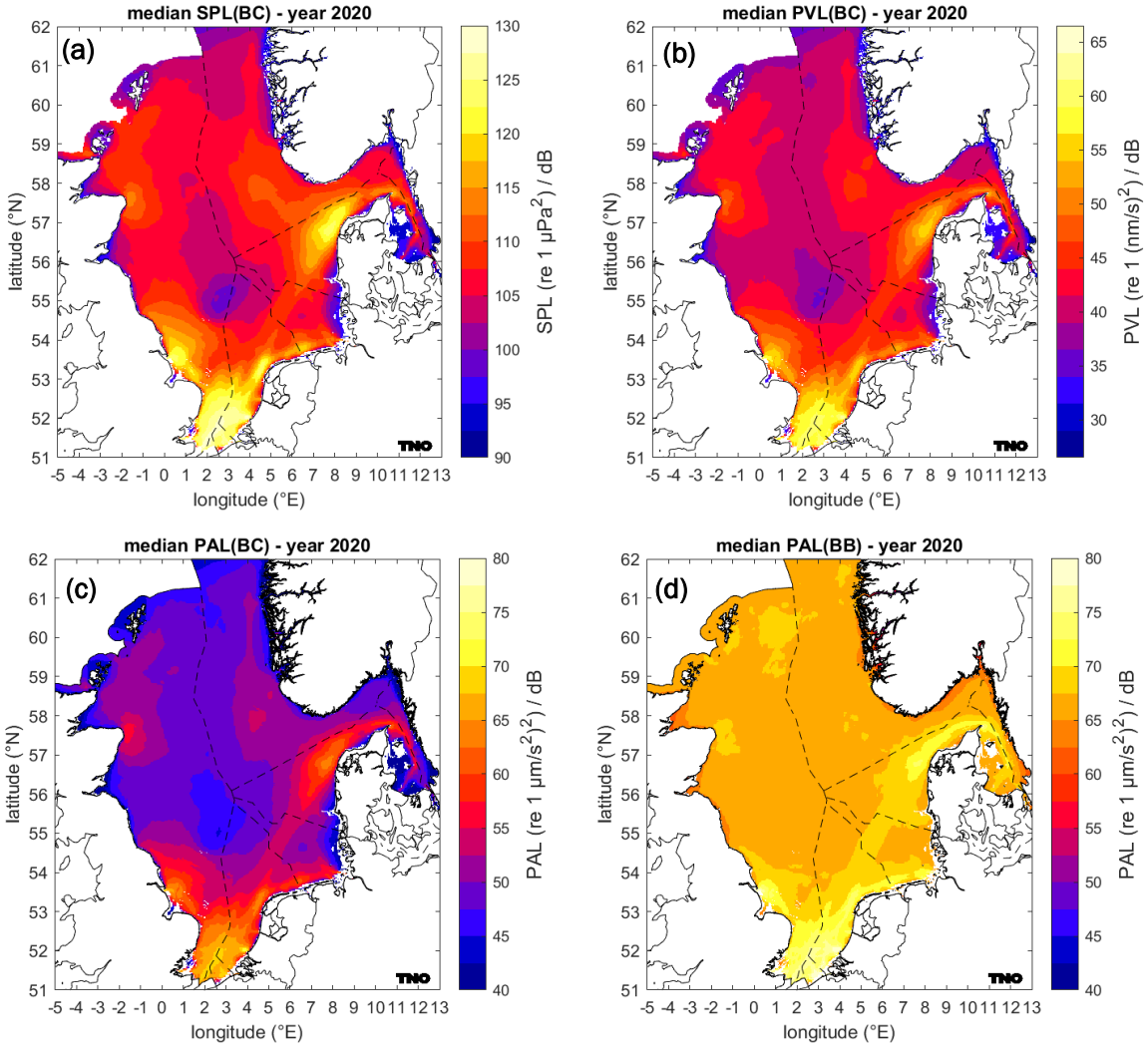

Figure 5-1: Maps of the annual median SPL (a), PVL (b) and PAL (BC = 8.91 Hz to 891 Hz) (c), and PAL (BB = 8.91 Hz to 22.4 kHz) from shipping and wind on the North Sea in 2020, see (de Jong C. , Binnerts, de Krom, & Gaida, 2022). The colour scale for the PVL map is scaled to that of the SPL maps, according to eq.(20).

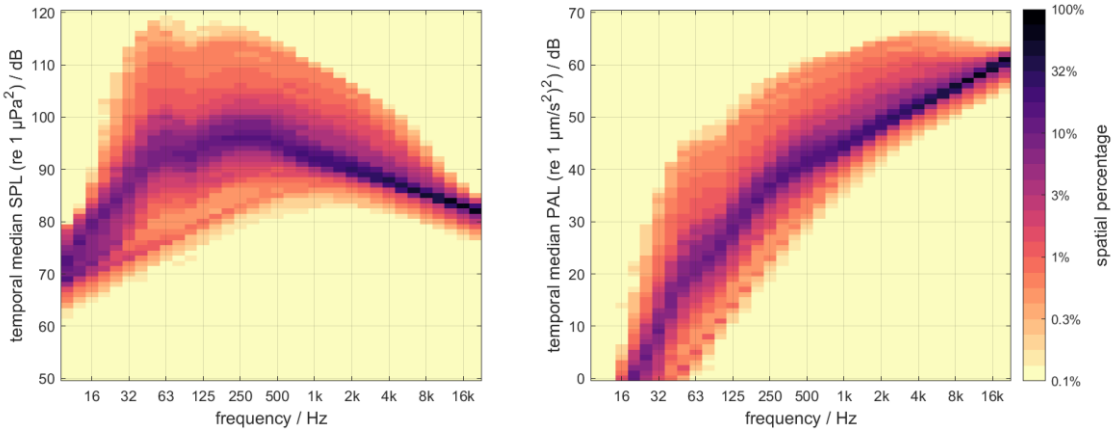

Figure 5-2: Spectrum of the annual median SPL (left) and PAL (right) in the maps (Figure 5-1). The colours indicate the percentage (logarithmic scale) of the area in which the levels occur.

5.2 Local sound maps for the Scheveningen area (Netherlands)

The extended modelling capability to calculate maps that represent sound particle motion was applied to an area of 10×10 km² around the sensor location for the measurement campaign offshore Scheveningen (The Netherlands), see §4.2 and Annex C. The particle motion maps were computed for ship traffic noise recorded over a period of three days during the particle motion sensor experiment (17/05 to 19/05/2022). Ship traffic at seas is monitored by AIS (Automatic Identification System) and VMS (Vessel Monitoring System) services. The local TNO AIS data recordings were used.

The following sections provide a description of the steps that lead to a calculation of maps of sound particle acceleration level (PAL) (based on the magnitude of the sound particle acceleration vector). It further shows a comparison of the directly calculated PAL maps with PAL maps obtained from modelling sound pressure level using the assumption of a scaled impedance of 1 (see section 2.6). In a last step the modelling results are compared with the sensor measurements.

5.2.1 Data preparation and processing

5.2.1.1 AIS data

For modelling particle motion and sound pressure of ship traffic, AIS data was retrieved via the local TNO portal[6] for the three days of sensor measurements (17/05 to 19/05/2022). The processing of the AIS data included filtering and interpolation of the individual ship trajectories to a regular temporal resolution of 10 minute time stamps. The interpolated ship trajectories are further filtered and checked for validity. The same filters as used in the Jomopans project are applied (de Jong C. , Binnerts, de Krom, & Gaida, 2022), such as speed filter, depth filter and vessel track filter. Vessel tracks with a speed lower than 0.5 kn and a speed higher than 50 kn were removed, vessels at a location with a water depth below 5 m were rejected. For each interpolated vessel entry the latitude and longitude, speed over ground, vessel class and length

[6] https://www.aishub.net/

were stored for the computation of the source level. Figure 5-3 shows the number of interpolated track entries per ship type and Figure 5-4 shows the interpolated ship densities.

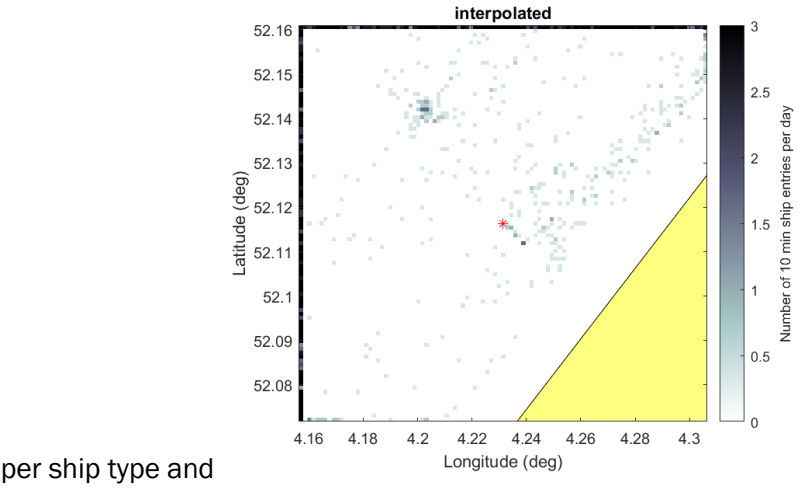

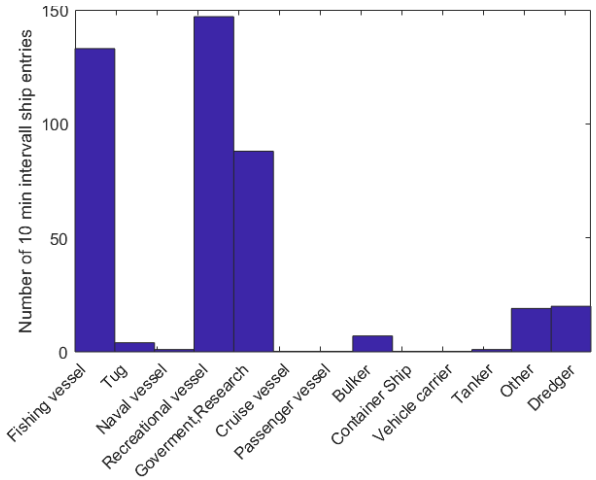

Figure 5-3 Distribution of interpolated ship entries (10 min temporal resolution) per ship class occurring in an area of 10 x 10 km around the sensor location from 17/05 to 19/05/2022. In total 422 ship entries are registered yielding 422 source locations for the sound particle motion simulations.

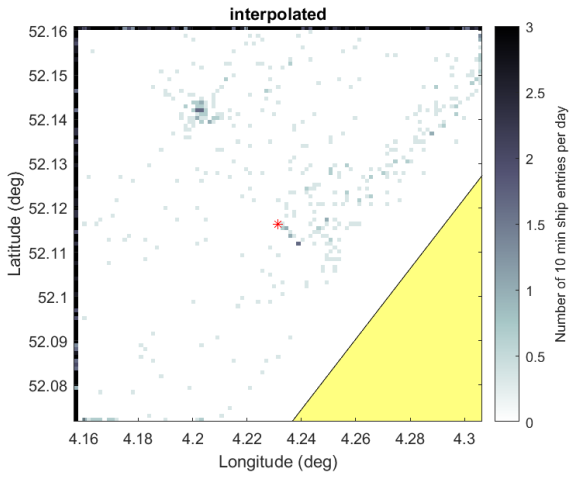

Figure 5-4 AIS data recorded from 17/05 to 19/05/2022, processed and interpolated on a regular temporal grid of 10 minute time stamps.

5.2.1.2 Jomopans-Echo ship source model

The Jomopans-Echo ship source model was employed to model the source level of the various ship types present in the investigated area (Figure 5-3) (MacGillivray & de Jong, 2021). This model calculates the ship source level spectrum, as a function of frequency, ship speed over ground, ship length and ship type (vessel class). The model is valid for a frequency range between 20 Hz and 20 kHz with a standard deviation of 6 dB.

5.2.1.3 Ship noise propagation model – RAM settings

The verified (§4.1) extension of RAM (PE) to model in addition to sound pressure propagation loss and particle motion propagation loss (see Annex A) was employed. For the RAM modelling, a split-step Padé solution method is used with 8 Padé terms and a range step of 6λ and a depth step of 0.1λ, with λ the wavelength in water (assuming a sound speed of 1500 m/s). The sediment is modelled in two layers. The upper layer contains a uniform sediment (see Table 1) and has a thickness of 20λ. The lower layer is a PML (perfectly matched layer) with a thickness of 158λ. The propagation loss modelling is carried out at the centre frequencies of the decidecade bands of the measurements, between 50 Hz and 4 kHz. This range extends a few bands beyond the frequency range (up to 1 kHz) considered of interest for impact on aquatic animals (§2.2). To estimate the mean propagation loss over the decidecade band, a range-averaging is applied, as suggested by (Harrison & Harrison, 1995). Arithmetic averaging of the received mean-square sound pressure and sound particle velocity over range bins with a relative width ($10^{-1/10}R_{\mathrm{centre}}$) corresponds with averaging over decidecade frequency bands.

The water depth along the trajectory between the source and receiver grid point is obtained from the EMODnet[7] 0.125 minute × 0.125 minute grid bathymetry map. The Map viewer – Geology (emodnet-geology.eu) rates the sediment in the area as 'sand' and 'coarse substrate', which is expected to be somewhere between gravel and sand. Hence, for the model calculations the acoustic properties of 'coarse sand' (median grain size 0 ϕ) were selected; Table 4.18 in (Ainslie M. , Principles of Sonar Performance Modeling, 2010), see Table 1Table C.2.

[7] https://www.emodnet-bathymetry.eu/

Table 1 RAM input parameters. Sediment sound speed c, density ρ, attenuation α, wavelength λ, and frequency f.

Water acoustic parameters (at seabed)	c_w = 1495.9 m/s ρ_w = 1021.5 kg/m³ absorption: (van Moll, Ainslie, & van Vossen, 2009)
Sediment type	Slightly gravelly Sand (Folk scheme) = Coarse sand: median grain size 0 ϕ (Ainslie M. , Principles of Sonar Performance Modeling, 2010)
Geoacoustic parameters	c_s = 1911.4 m/s (frequency independent) ρ_s = 2363.8 kg/m³ $\alpha\lambda$ = 0.87 dB
Frequencies	f = 50 to 4000 Hz (decidecade band centre frequencies)
Source depth	6 m

5.2.1.4 Map generation

Numerical modelling of underwater soundscape maps requires selection of a model resolution in space, time and frequency. A detailed description of the full process is described in the Jomopans modelling guidelines (de Jong C. , Binnerts, Robinson, & Wang, 2021).

Spatial resolution

For the sound particle motion maps, the depth averaged mean square sound particle acceleration was calculated between modelled values at the seabed and 1 m below the sea surface. The horizontal resolution of the receiver grid was set to 100 x 100 m². The receiver grid encloses an area of 10 x 10 km² around the sensor location where the grid points are the geographical locations for computing the PAL.

Frequency resolution

The modelling was carried out for a frequency range from 50 Hz to 4 kHz corresponding to the frequency range of the measurements. The acoustic modelling in the frequency domain is applied to single frequencies. Since the acoustic metrics are represented in decidecade frequency bands, the centre frequency of each band was chosen for the modelling. This is a substantial reduction of the calculation effort. A sensitivity study in the Jomopans project (de Jong C. , et al., 2021)has estimated the uncertainty in the calculated depth averaged SPL related to using one frequency per decidecade band to be approximately 2 dB.

Source positions and spatial processing of particle motion map

The considered time period was relative short with three days and the area relatively small with an extent of 10 x 10 km². This yielded to 422 ship entries. Therefore, it was feasible to calculate the propagation loss from the location of the ship entry instead of creating a source grid, as it was done for the North Sea sound maps in the Jomopans project, to reduce computation time.
Also, to reduce the complexity of computing the propagation loss from each source to each receiver grid point, sound maps are generally obtained by means of two-dimensional linear interpolation between radial transects (slices/radials) from each source. The required number of radials

depends on the spatial variability of the environment. In Jomopans, it was shown that a decrease from 36 to 16 radials (uniformly distributed over 360˚) has a small effect (< 1 dB) on the predicted SPL for the majority of the North Sea (de Jong C. , Binnerts, de Krom, & Gaida, 2022). For the Scheveningen area, being closer to the coastline resulting in more bathymetric variation (water depth between 5 and 20 m), 36 radials were used. The maximum radial length was set to 7 km. In case the land or a water depth shallower than 5 m was reached within a range of 7 km, the radial length was reduced.

5.2.1.5 Summary of computational steps

Each 10 min ship position was considered as a source and in combination with the ship length, speed and type the source level (SL) was computed using the Jomopans source level echo model. For each source position $x_{\mathrm{src}}, y_{\mathrm{src}}$ at time stamp t_i, the PL, PAPLr and PAPLz were modelled in the radial direction. The PL, PAPLr and PAPLz were depth averaged and then 2D interpolated on the receiver grid. The SPL, PALr and PALz were computed for each receiver grid in position x_{rec}, y_{rec}, time stamp t_i and decidecade center frequency f via

$$
\begin{aligned}
L_p(x_{\mathrm{rec}}, y_{\mathrm{rec}}, f, t_i) &= L_s(x_{\mathrm{src}}, y_{\mathrm{src}}, f, t_i) - N_{\mathrm{PL},p}(x_{rec}, y_{rec}, x_{src}, y_{src}, f) \\
L_{a_r}(x_{\mathrm{rec}}, y_{\mathrm{rec}}, f, t_i) &= L_s(x_{\mathrm{src}}, y_{\mathrm{src}}, f, t_i) - N_{\mathrm{PL},a_r}(x_{rec}, y_{rec}, x_{src}, y_{src}, f) \\
L_{a_z}(x_{\mathrm{rec}}, y_{\mathrm{rec}}, f, t_i) &= L_s(x_{\mathrm{src}}, y_{\mathrm{src}}, f, t_i) - N_{\mathrm{PL},a_z}(x_{rec}, y_{rec}, x_{src}, y_{src}, f)
\end{aligned}
$$

This results in N_s x N_f layers of receiver grids with an interpolated SPL and PALr and PALz. N_s is the number of ship entries (time t_i and location $x_{\mathrm{src}}, y_{\mathrm{src}}$) within the three days in the area of 10 x 10 km² around the rig and N_f is the number of decidecade frequencies. The magnitude of the particle acceleration PAL was computed from the radial and vertical acceleration via

$$
L_{\mathrm{a}} = 10 \log_{10}\left(10^{\frac{L_{a_r}}{10\ \mathrm{dB}}} + 10^{\frac{L_{a_z}}{10\ \mathrm{dB}}}\right) \mathrm{dB}
$$

The contributions from ship entries were incoherently summed per time stamp. A broadband SPL and PAL were computed by incoherently summing the mean-square sound pressure and sound particle acceleration respectively over the decidecade frequency bands. For the final maps, the spatial distribution of a temporal arithmetic mean, and the 50th (median) and 90th percentiles of the calculated broadband SPL and PAL were computed over the three days.

5.2.2 Results

5.2.2.1 Sound maps

Figure 5-5 shows the calculated maps of the median value over the three days of the 10-min snapshots of the broadband SPL and PAL in the selected area.

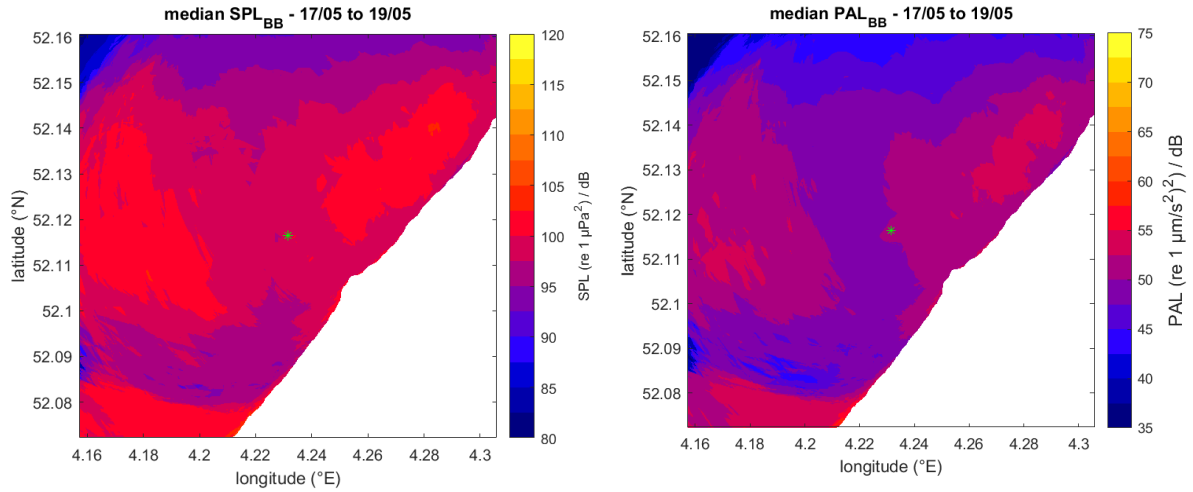

Figure 5-5 Maps of a 3 day median broadband SPL (a) and PAL (c), from shipping in an area of 10 x 10 km² around the rig location (green asterisk in the centre). The white area in the graph represents land as well as water depths less than 5 m. The colour scale spans 40 dB, with the maximum value determined to include the highest values in the map.

Figure 5-6 shows maps of the 90th percentile over the three days of the 10-min snapshots of the broadband SPL and PAL in the selected area. This illustrates that the highest levels occur along the north-north-west shipping track from the port of Scheveningen, during 10% of the time.

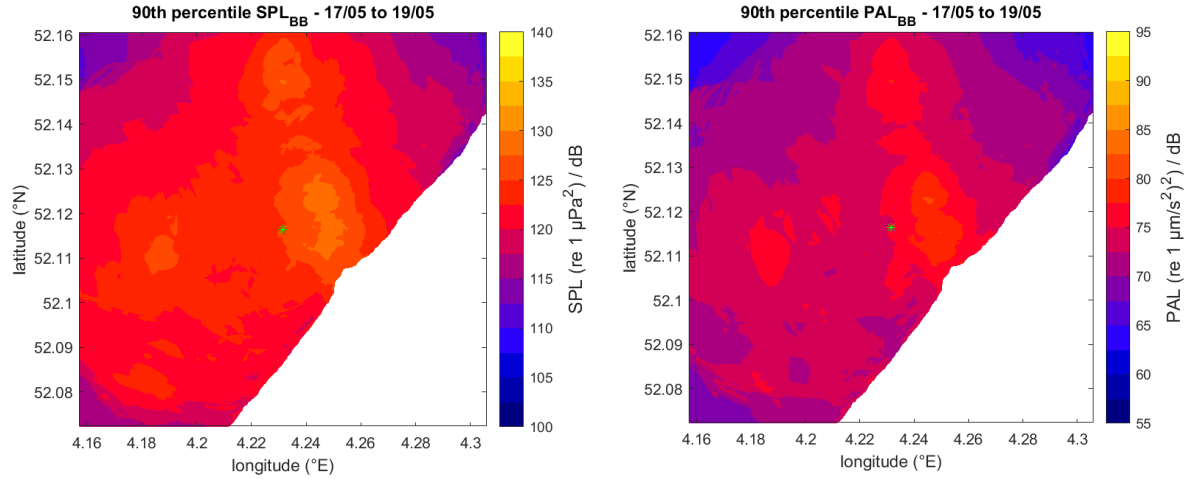

Figure 5-6 Maps of a 3 day 90th percentile broadband SPL (a) and PAL (c), from shipping in an area of 10 x 10 km² around the rig location (green asterisk).

Figure 5-7 shows the arithmetic mean broadband SPL and PAL over the three days in the selected area. The highest mean levels appear along the track from and to the port, occurring 10% of the time.

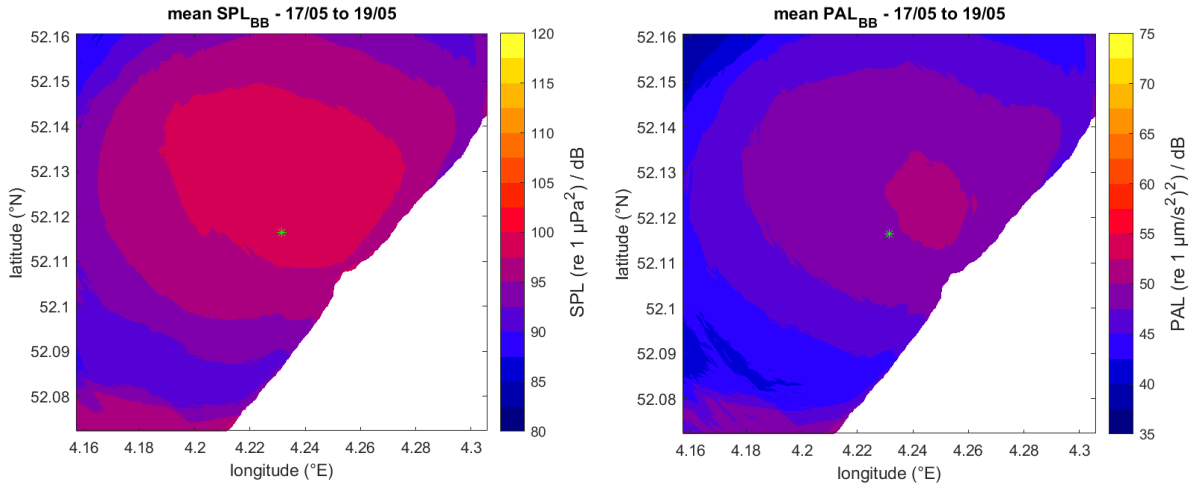

Figure 5-7 Maps of a 3 day mean broadband SPL (a) and PAL (c), from shipping in an area of 10 x 10 km² around the rig location (green asterisk).

5.2.2.2 Sound level spectra

Figure 5-8 shows the spectra of the temporal median SPL and PAL in the area, expressed as spatial probability density, representing the percentage of the area in which these levels occur. This illustrates that the PAL peaks at higher frequencies than the SPL. The relevance of the spectral shape depends on the evaluation of the received spectrum, which will possibly include frequency weighting. This will become clearer if more information on the sensitivity of aquatic species to sound comes available in the future.

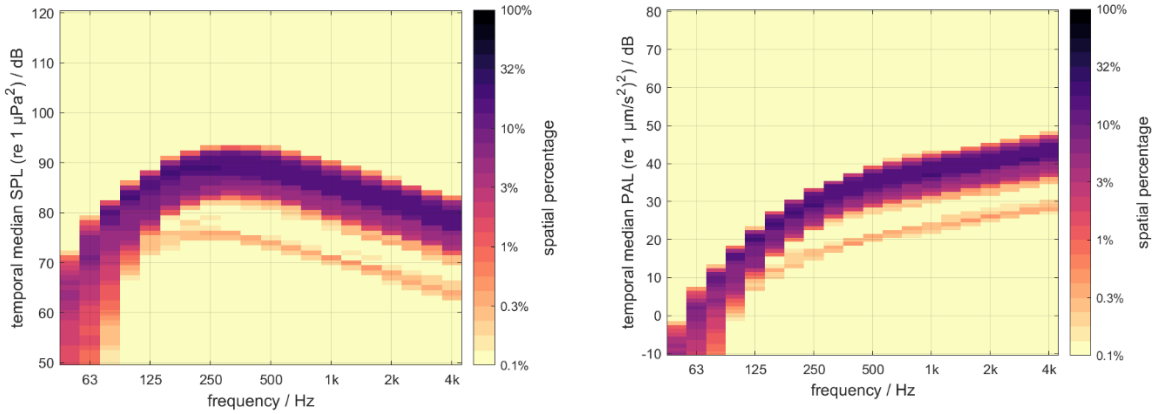

Figure 5-8 Spectra of the spatial probability density of the 3 day median SPL (left) and PAL (right) in the maps (Figure 5-5). The colours indicate the percentage (logarithmic scale) of the area in which the levels occur.

5.2.2.3 Comparison with measurements

Sound map snapshots were calculated at the 10-min time stamps when there were ship AIS entries within the selected area (10 x 10 km²). The calculated SPL and PAL spectra at the location of the vector sensor rig at these time stamps are compared with the measured SPL and PAL snapshots (1-s averaging time) at the same time stamps. Because the Jomopans-ECHO ship source level model is a statistical model, with a statistical uncertainty of 6 dB, the comparison is made statistically as well. Figure 5-9 shows the temporal probability (over the 422 registered events,

Figure 5-3) of the modelled and measured SPL spectra at the rig location, and Figure 5-10 shows the temporal probability for the PAL. The comparison is complicated by the lower limit of the measured spectra, caused by non-modelled contributions to the measured sound spectra from distant ships, breaking waves and surf, flow noise and system self-noise. Generally the highest levels, from the closets passing ships, appear to be overestimated, but a quantitative statistical assessment of the model-data comparison would require a longer recording period, with more ship passages.

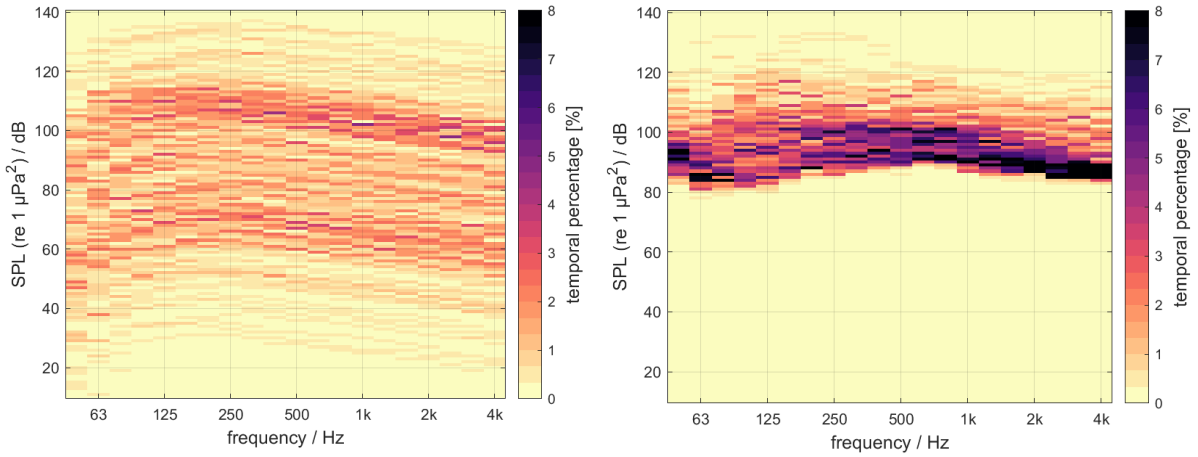

Figure 5-9 Spectra of the temporal probability density of the modelled SPL (left) and measured SPL (right) at the rig over the time period of around 3 days (model: 17-5-2021 00:00 until 19-5-2021 24:00; measurements 17-5-2021 07:50 until 19-5-2021 24:00). The colours indicate the percentage (linear scale) of the 10 min interval time stamps in which the levels occur.

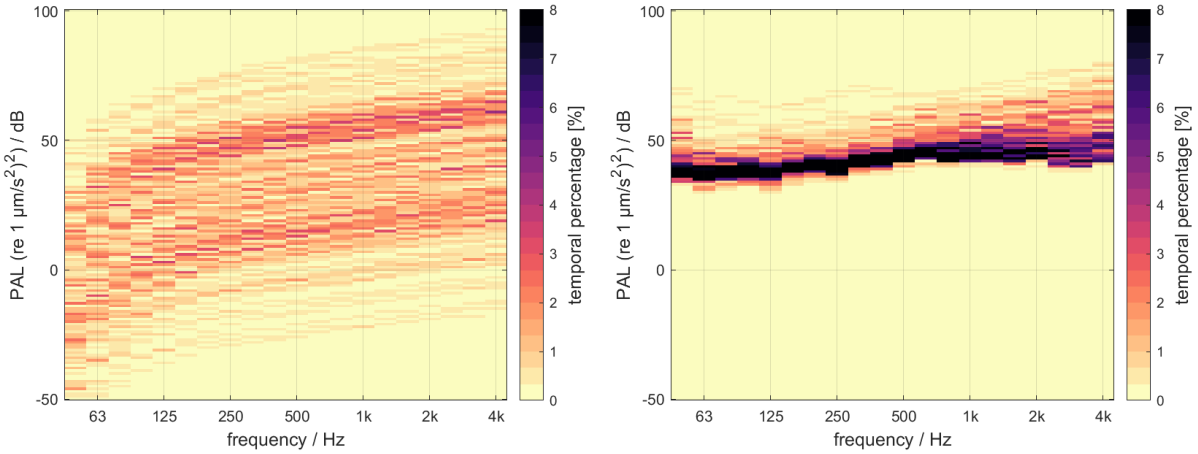

Figure 5-10 Spectra of the temporal probability density of the modelled PAL (left) and measured PAL (right) at the rig over the time period of around 3 days. The colours indicate the percentage (linear scale) of the 10 min interval time stamps in which the levels occur.

5.2.2.4 Calculating PAL from SPL

As explained in sections 2.6 and 4.1.1, and illustrated in section 5.1, the PAL map can be calculated by scaling the SPL maps to PVL maps, using the characteristic specific impedance of the fluid according to eq.(20), and then calculating PAL from PVL using eq.(21).

Figure 5-11 shows the difference between the PAL map directly calculated using the RAM model and the PAL map calculated from the SPL. The circular shapes that appear in the difference plots around certain ship locations are related with the spatial discretization of the model. For these maps of the depth-averaged broadband PAL the difference is negligible (<1 dB at all locations), confirming that the calculation of PAL from SPL is valid.

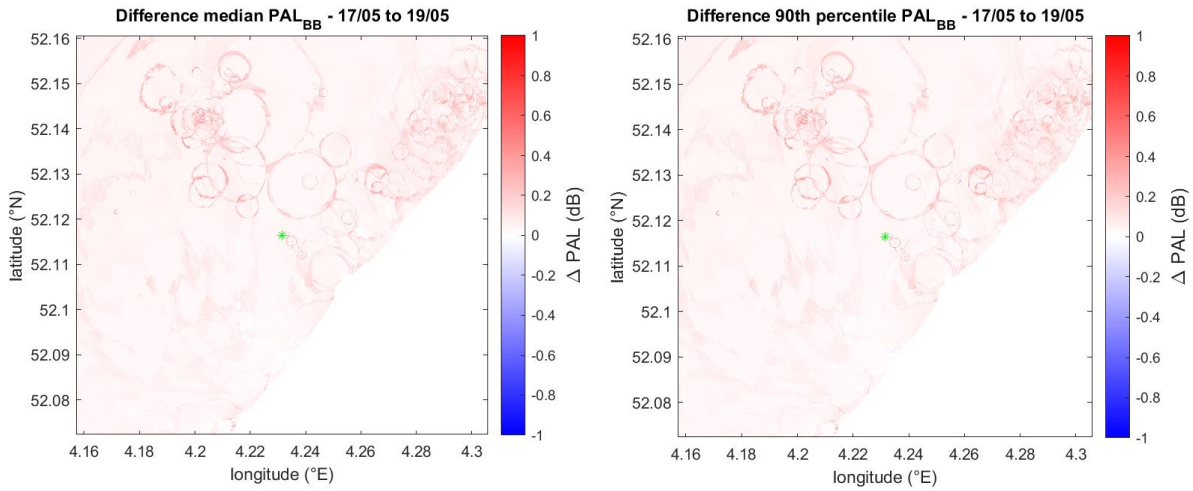

Figure 5-11 Difference plot between PAL map computed directly with RAM and PAL map retrieved from SPL map using scaled impedance of 1.

6 Guidelines for sound particle motion mapping

This study has explored the steps to be taken for the creating of spatial maps of sound particle motion metric. This leads to the following recommended approach. The examples ('e.g.') are provided to illustrate possible choices and are not to be interpreted as guidelines.

6.1 Problem definition

The first step is to specify the required particle motion maps. This involves selection of:

- Project area (e.g. North Sea)
- Spatial resolution (e.g. 0.05° longitude × 0.025° latitude grid)
- Spatial observation window (e.g. depth average at grid locations)
- Time period (e.g. May 2020)
- Temporal resolution (e.g. one map 'snapshot' per 10 minute)
- Temporal observation window (e.g. 1 minute, or 'steady state', see Chapter 3)
- Sound particle motion metric (e.g. monthly PAL, or monthly percentiles of PAL snapshots)
- Frequency range (e.g. 20 Hz to 20 kHz decidecade bands)
- Sound sources to be considered in the modelling (e.g. ships from AIS)

6.2 Select modelling approach

The next step is to select the appropriate models for:

- Source level (e.g. Jomopans-Echo ship source level model, or a wind noise model)
- Propagation loss (e.g. RAM parabolic equation model)[8]

The selection of the propagation loss model also requires specification of:

- Spatial modelling approach (e.g. source to receiver grid, or $N \times 2\mathrm{D}$ approach and interpolation to receiver grid)
- Model settings (e.g. for RAM: a split-step Padé solution with 8 Padé terms)
- Model spatial settings (e.g. 16 radial transects per source, with a horizontal resolution of 100 m, to a maximum distance of 400 km. PAL averaged over 10 receiver depths per transect position and then linearly interpolated to receiver grid positions)

It is essential to be able to demonstrate that the applied models have been verified and, where possible, validated (see Chapter 4).

The selected sound particle motion metric can be modelled directly by a propagation model that includes this option (e.g. the models summarized in §4.2). For maps of the depth-averaged PVL or PAL it can be estimated from the sound particle velocity obtained by dividing the calculated sound pressure by the characteristic specific impedance of the fluid. The latter approach is acceptable at distances greater than about a quarter wavelength from the air-water interface and the seabed, and about one wavelength from the sound sources, or about three water depths if the water depth is smaller than the wavelength.

[8] The calculation of PAL from wind noise has not yet been verified or validated.

6.3 Select model input data

Dependent of the selected models, various sets of input data need to be obtained. The origin of the data needs to be specified. This includes, for example:

- Bathymetry (e.g. EMODnet[9] 0.125 minute × 0.125 minute grid), corrected for tide when and where required.
- Sediment properties (e.g. based on the Folk scale provided at EMODnet[10], with the conversions proposed in Chapter 4 of (Ainslie M. , Principles of Sonar Performance Modeling, 2010)).
- Water properties (e.g. temperature and salinity from CMEMS[11], to calculate sound speed profiles where required)
- For shipping noise maps: ship AIS data such as ship type, ship length (overall), latitude, longitude and speed (over ground), at the map snapshot times. This may require temporal and spatial interpolation, as well as parameter checks, to correct for erroneous or missing parameters.
- For wind noise maps: wind speed at a specified height above the water surface (e.g. from CMEMS[11]).

6.4 Perform model calculations

Depending on the problem definition (number of locations, time steps, and frequencies) the calculations can require a lot of computer memory and time. Hence, the model calculations need to be carefully planned.

6.5 Back up data

The model calculations need to be traceable. This requires making a backup of the model results together with the applied input parameters and model settings.

6.6 Reporting

The value of the calculated sound maps depends on a clear description of the presented metrics and applied models and inputs. Here are some general reporting guidelines, see also (Nedelec, et al., 2021):

- Follow and cite ISO 18405 for basic terminology. Define new terms where needed.
- When reporting a level in decibels
    - Identify the quantity (must be a power quantity or a root-power quantity)
    - State the reference value in SI units
- Specify the mapped metric(s), including all aspects mentioned in §6.1.
- Describe the applied models and model settings (§6.2) and input parameters (§6.3).

[9] https://www.emodnet-bathymetry.eu/

[10] https://emodnet.ec.europa.eu/geoviewer/

[11] https://data.marine.copernicus.eu/product/GLOBAL_ANALYSISFORECAST_PHY_001_024/description

- When plotting graphs and sound maps use a colourblind-friendly palette and clearly distinguishable markers.

6.7 Open issues

This report provides the first approach for producing sound particle motion maps, including verification and validation of some of the underlying models. Further development and testing of the proposed approach is recommended. Issues that have not or insufficiently been addressed include:

- Reduce uncertainty in the geo-acoustic parameters and modelling for the propagation loss modelling, This could include adding depth-dependence in the sediment properties (gradient and/or layering) and adding sediment shear properties in the modelling, at the cost of an increased computational effort.
- Extend the modelling capability to shallower (<10 m depth) and deeper (>200 m depth) water. Extension towards shallower water is mainly limited by uncertainty in the geoacoustic modelling, Extension towards deeper water would require including effects of depth-dependence (sound speed profile) in the propagation loss models.
- Reduce uncertainty in the source models and input data. For shipping noise this concerns enhancing the input data beyond what can currently be obtained from AIS. This includes using other traffic information sources (such as VMS) and or satellite images to add missing ships as well as coupling with technical databases to allow for more detailed modelling of the ship source level, such as proposed in (Wittekind, 2014) and (Lloyd, Daniel, Bosschers, & Schuster, 2024).
- Exploring the possibilities for mapping particle motion vectors. In contrast with sound pressure, sound particle motion includes information about the direction in which the sound is propagating.
- Acquiring more measurements for model validation.
- Modelling sound particle motion in bounded environments, such as laboratory tanks and aquaria. The finite-element modelling approach (§3.2.2) is considered suited for this application, but this has not been tested in the scope of this study.

7 References

Ainslie, M. (2010). *Principles of Sonar Performance Modeling.* Springer-Praxis.

Ainslie, M., Bruliard, F.-A., de Jong, C., Díaz, J., Folegot, T., Ghasemi, M., . . . van der Schaar, M. (2024). *SATURN Acoustical Terminology Standard.* SATURN Deliverable 2.3.

Ainslie, M., Harrison, C., & Zampolli, M. (2011). An analytical solution for signal background and signal to background ratio for a low frequency active sonar in a Pekeris waveguide satisfying Lambert's rule. *Proc. 4th International Conference and Exhibition on "Underwater Acoustic Measurements: Technologies & Results".* Kos, Greece.

Ainslie, M., Miksis-Olds, J., Heaney, K., de Jong, C., von Benda-Beckmann, A., & Lyons, A. (2018). *ADEON Underwater Soundscape and Modeling Metadata Standard. Version 1.0.* Technical report by JASCO Applied Sciences for ADEON Prime Contract No. M16PC00003.

Binnerts, B., de Jong, C., Karasalo, I., Östberg, M., Folegot, T., Clorennec, D., . . . Wang, L. (2019). Model benchmark solutions for ship noise in shallow water. *Proc. UACE 2019.*

Chapman, C., & Hawkins, A. (1973). A field study of hearing in the cod, Gadus morhua L. *J. Comp. Physiol., 85*, 147-167.

Chapman, C., & Sand, O. (1974). Field studies of hearing in two species of flatfish, Pleuronectes platessa (L.) and Limanda limanda (L.) (Family Pleuronectidae). *Comp. Biochem. Physiol., 47A*, 371-385.

Collins, M. (1990). The rotated parabolic equation and sloping ocean bottoms. *J. Acoust. Soc. Am., 87*(3), 1035-1037.

Collins, M. (1993). A split-step Padé solution for the parabolic equation method. *J.Acoust.Soc.Am., 93*, 1936-1942.

Collins, M., & Evans, R. (1992). A two-way parabolic equation for acoustic backscattering in the ocean. *J. Acoust. Soc. Am., 91*(3), 1357-1368.

Davies, D. (1965). Dispersed Stoneley waves on the ocean bottom. *Bulletin of the Seismological Society of America, 55*(5), 903-918.

de Jong, C., Binnerts, B., de Krom, P., & Gaida, T. (2022). *North Sea Sound Maps 2019-2020.* Report of the EU INTERREG Joint Monitoring Programme for Ambient Noise North Sea (Jomopans).

de Jong, C., Binnerts, B., Östberg, M., Karasalo, I., Folegot, T., Clorenneq, D., . . . Wang, L. (2021). *Jomopans model benchmarking and sensitivity studies.* Report of the EU INTERREG Joint Monitoring Programme for Ambient Noise North SEA (JOMOPANS).

de Jong, C., Binnerts, B., Robinson, S., & Wang, L. (2021). *Guidelines for modelling ocean ambient noise. Report of the EU INTERREG Joint Monitoring Programme for Ambient Noise North Sea (Jomopans).* The Hague: TNO.

Felsen, L. (1987). Numerical solutions of two benchmark problems. *J.Acoust.Soc.Am. Suppl. 1, 81*, S39.

Felsen, L. (1989). Benchmarks: An option for quality assessment. *J.Acoust.Soc.Am., 87*, 1497-1498.

Gray, M., Rogers, P., & Zeddies, D. (2016). Acoustic particle motion measurement for bioacousticians: principles and pitfalls. *Proc. Mtgs. Acoust., 27*(010022).

Harrison, C., & Harrison, J. (1995). A simple relationship between frequency abd range averages for boradband sonar. *J. Acoust. Soc. Am, 97*(2), 1314-1317.

Hawkins, A., & Johnstone, A. (1978). The hearing of the Atlantic salmon, Salmo salar. *J.Fish.Biol., 13*, 655-673.

Hawkins, A., Johnson, C., & Popper, A. (2020). How to set sound exposure criteria for fishes. *The Journal of the Acoustical Society of America, 147*(3), 1762-1777.

International Organization for Standardization. (2017). *Underwater acoustics - Terminology (ISO 18405).* Retrieved from https://www.iso.org/obp/ui/#iso:std:iso:18405:ed-1:v1:en

ISO. (2017). *ISO 18405 Underwater acoustics - Terminology.* Geneva, Switzerland. Retrieved from https://www.iso.org/obp/ui/#iso:std:iso:18405:ed-1:v1:en

ISO/IEC 25002. (2024). *Systems and software engineering — Systems and software Quality Requirements and Evaluation (SQuaRE) — Product quality model.* Geneva: ISO/IEC.

Jansen, E., Prior, M., & Brouns, E. (2019). On the conversion between sound pressure and particle motion. *Proc. Mtgs. Acoust., 37.*

Jensen, F., & Ferla, C. (1990). Numerical solutions of range-dependent benchmark problems in ocean acoustics. *J.Acoust.Soc.Am., 87*(4), 1499-1510.

Jensen, F., Kuperman, W., Porter, M., Schmidt, H., & Tolstoy, A. (2011). *Computational ocean acoustics.* New York: Springer New York.

Küsel, E., & Siderius, M. (2019). Comparison or propagation models for the characterization of sound pressure fields. *IEEE Journal of Oceanic Engineering, 44*(3), 598-610.

Lloyd, T., Daniel, J., Bosschers, J., & Schuster, M. (2024). PIANO: A physics-based semi-empirical source level model for fleet-scale ship URN prediction. *Eighth International Symposium on Marine Propulsors.* Berlin.

Ludwig, W. (1970). Seismic refraction. *The Sea, 4*, 53-84.

MacGillivray, A., & de Jong, C. (2021). A Reference Spectrum Model for Estimating Source Levels of Marine Shipping Based on Automated Identification System Data. *J. Mar. Sci. Eng., 9*, 369.

Murphey, J., & Chin-Bing, S. (1989). A finite-element model for ocean acoustic propagation and scattering. *J.Acoust.Soc.Am., 86*(4), 1478-1483.

Nedelec, S., Ainslie, M., Andersson, M., Cheong, S., Halvorsen, M., Linné, M., . . . Ward, J. (2021). *Best Practice Guide for Underwater Particle Motion Measurement for Biological Applications.* Technical report by Exeter University for the IOGP Marine Sound and Life Joint Industry Programme.

Nedelec, S., Campbell, J., Radford, A., Simpson, S., & Merchant, N. (2016). Particle motion: the missing link in underwater acoustic ecology. *Methods in Ecology and Evolution*. doi:0.1111/2041-210X.12544

Oppeneer, V., de Jong, C., Binnerts, B., Wood, M., & Ainslie, M. (2023). Modelling sound particle motion in shallow water. *J. Acoust. Soc. Am., 154*(6), 4004–4015.

Pekeris, C. (1948). Theory of propagation of explosive sound in shallow water. *Mem.-Geol.Soc.Am., 27*.

Pierce, A. (2019). *Acoustics – An Introduction to Its Physical Principles and Applications* (3rd ed.). ASA Press, Springer.

Popper, A., Hawkins, A., Fay, R., Mann, D., Bartol, S., Carlson, T., . . . Tavolga, W. (2014). *Sound Exposure Guidelines (ASA S3/SC1.4 TR-2014).*

Putland, R., de Jong, C., Binnerts, B., Farcas, A., & Merchant, N. (2022). Multi-site validation of shipping noise maps using field measurements. *Marine Pollution Bulletin, 179*(113733).

Robinson, S., & Wang, L. (2021). *Terminology for ocean ambient noise.* Report of the EU INTERREG Joint Monitoring Programme for Ambient Noise North Sea (Jomopans).

Schmidt, H., & Jensen, F. (1985). A full wave solution for propagation in multi-layered viscoelastic media with application to Gaussian beam reflection at fluid-solid interfaces. *J.Acoust.Soc.Am., 77*(3), 813-825.

Sertlek, H., & Ainslie, M. (2014). A depth-dependent formula for shallow water propagation. *J.Acoust.Soc.Am., 136*(2), 573-582.

Sertlek, H., Ainslie, M., & Heaney, K. (2018). Analytical and numerical propagation loss predictions for gradually range-dependent isospeed waveguides. *IEEE Journal of Oceanic Engineering, 44*(4), 1240-1252.

Sertlek, H., Slabbekoorn, H., Ten Cate, C., & Ainslie, M. (2019). Source specific sound mapping: Spatial, temporal and spectral distribution of sound in the Dutch North Sea. *Environmental pollution, 247*, 1143-1157.

Southall, B. L., Finneran, J. J., Reichmuth, C., Nachtigall, P., Ketten, D., Bowles, A. E., . . . Tyack, P. L. (2019). Marine Mammal Noise Exposure Criteria:Updated Scientific Recommendations for Residual Hearing Effects. *Aquatic Mammals*, 125-232.

van Moll, C., Ainslie, M., & van Vossen, R. (2009). A Simple and Accurate Formula for the Absorption of Sound in Seawate. *IEEE Journal of Oceaniic Engineering, 34*(4).

Wittekind, D. K. (2014). A simple model for the underwater noise source level of ships. *Journal of Ship Production and Design, 30*(1), 7-14.

Zhang, Z., & Tindle, C. (1995). Improved equivalent fluid approximations for a low shear speed ocean bottom. *J.Acoust.Soc.Am, 98*(6), 3391-3396.

Zhou, J.-X., Zhang, X.-Z., & Knobles, D. (2009). Low-frequency geoacoustic model for the effective properties of sandy sea bottoms. *J. Acoust. Soc. Am., 125*(5), 2847-2866.

Annex A – Calculating particle motion from sound pressure

Sound propagation models generally compute the sound pressure spectrum $P(r,z,f)$ due to a (unit) source sound pressure spectrum $P_S(f)$, as a function of range r, depth z and frequency f. The radial and vertical components of sound particle acceleration (A_r and A_z) are related to the pressure gradients:

$$A_r = -\frac{1}{\rho}\frac{\partial P}{\partial r} \quad \text{and} \quad A_z = -\frac{1}{\rho}\frac{\partial P}{\partial z} \tag{A.1}$$

The sound particle motion components follow from integration of the sound particle acceleration in the time domain. In the frequency domain this corresponds with:

$$V_r = \frac{A_r}{\mathrm{i}2\pi f} = -\frac{1}{\mathrm{i}2\pi f\rho}\frac{\partial P}{\partial r} \quad \text{and} \quad V_z = \frac{A_z}{\mathrm{i}2\pi f} = -\frac{1}{\mathrm{i}2\pi f\rho}\frac{\partial P}{\partial z} \tag{A.2}$$

In numerical model implementations, the spatial domain is then discretized in regular grids with $\boldsymbol{r} = r_i\hat{r} + z_j\hat{z}$, where i is the range index from 1 to I such that $r_1 = 0$, and $r_I = r_{\max}$, and j is the depth index from 1 to J such that $z_1 = 0$, and $z_J = z_{\max}$.

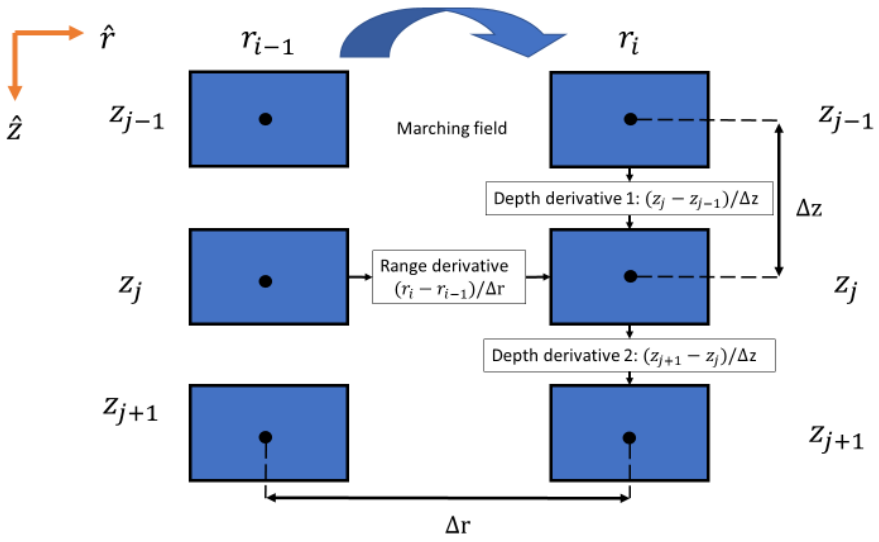

Figure A.1: Computing derivatives in a uniform grid. In range cells are separated by a distance Δr, in depth cells are separated by a distance Δz. The depth average in grid z_j can be estimated by the average between the upper and lower derivative.

In PE-codes such as RAM, the calculations are marching from range step $i-1$ to range step i. It is computationally efficient to estimate the range derivative at the edge between r_{i-1} and r_i and then calculate the depth derivative as the average of the interface between cell (r_i, z_{j-1}), (r_i, z_j) and the interface (r_i, z_j), (r_i, z_{j+1}). Working out the expressions, this leads to the following finite difference approximations:

$$\frac{\partial P(r,z,f)}{\partial r} \approx \frac{P(r_i,z_j,f) - P(r_{i-1},z_j,f)}{\Delta r} + O(\Delta r) \tag{A.3}$$

$$\frac{\partial P(r,z,f)}{\partial z} \approx \frac{P(r_i,z_{j+1},f) - P(r_i,z_{j-1},f)}{2\Delta z} + O(\Delta z^2) \tag{A.4}$$

The derivatives can also be calculated from pressure data at the points r_{i+1}. Except for the last range point, the pressure derivative with respect to range can then be approximated by

$$\frac{\partial P(r,z,\omega)}{\partial r} \approx \frac{P(r_{i+1},z_j,\omega)-P(r_{i-1},z_j,\omega)}{2\Delta r} + O(\Delta r^2) \quad \text{(A.5)}$$

whose truncation error scales with $O(\Delta r^2)$ instead of $O(\Delta r)$.

Annex B – Sound particle motion model benchmark

Because reference solutions are generally lacking, a comparison of different model solutions to the same problem is an accepted means to confirm the validity of numerical models (Felsen, 1989). This work builds on recent efforts for benchmarking models for the sound pressure field (Collins, 1990) (Collins & Evans, 1992) (Sertlek, Ainslie, & Heaney, 2018) (Binnerts, et al., 2019) (Küsel & Siderius, 2019).

This model benchmark is published in (Oppeneer, de Jong, Binnerts, Wood, & Ainslie, 2023).

B.1 Benchmark scenarios

Three different shallow-water sound propagation scenarios are provided. The geometry is sketched in figure B.1 and the model parameters for the geometry and the environmental properties for these scenarios are shown in table B.1.

Table B.1: parameters for the three benchmark scenarios

Scenario	Symbol	unit	I	II	III
Water depth	H	m	50	50	200 - 0
Source depth	D	m	5	5	100
Maximum range	R	km	10	10	4
Water density	ρ_w	kg/m³	1000	1000	1000
Water sound speed	c_w	m/s	1500	1500	1500
Sediment density	ρ_s	kg/m³	2000	2000	2000
Sediment compressional wave speed	c_c	m/s	1700	1700	1700
Sediment shear wave speed	c_s	m/s	0	700	0
Sediment compressional wave attenuation	$\alpha_c \cdot \lambda_c$	dB	0.5	0.5	0.5
Sediment shear wave attenuation	$\alpha_s \cdot \lambda_s$	dB	-	0.5	-

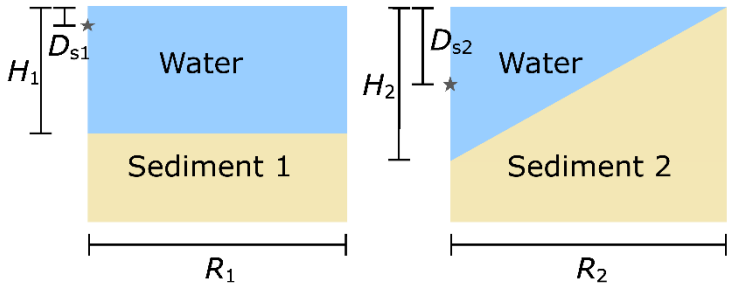

Figure B.1: Left: range-independent environment for scenarios I and II, right: range-dependent environment for scenario III (ASA wedge). The parameters are given in Table B.1.

The scenarios are described below. Three frequencies are considered for the sound propagation calculations for each scenario: 25, 100, and 400 Hz.

Scenario I: Range-independent waveguide with a fluid sediment
The first scenario is for a range-independent Pekeris waveguide (Pekeris, 1948). The same scenario has been used for recent benchmarks for sound pressure field models (Sertlek & Ainslie, 2014) (Binnerts, et al., 2019) (Küsel & Siderius, 2019). The water has a uniform depth of 50 m and the seabed is modelled as a fluid, only supporting compressional waves, with the properties of a 'sandy' sediment (Ainslie, 2010). The sound source is at 5 m depth below the water surface. This is a representative scenario for, for example, a merchant vessel in the North Sea (de Jong C. , et al., 2021).

Scenario II: Range-independent waveguide with a solid sediment
The geometry for the second scenario is the same as that of the first scenario, but in this case the seabed supports shear waves as well as compressional waves. The shear properties are tabulated in Table 1 and represent a rock with a low shear speed (Davies, 1965) (Ludwig, 1970).

Scenario III: Range-dependent waveguide with a fluid sediment
The third scenario is for a range-dependent waveguide (Jensen & Ferla, 1990). This scenario is the 'ASA wedge' benchmark case (Felsen, 1987), in which the water depth decreases from 200 m to 0 m over a distance of 4 km. The sound source is placed at 100 m below the water surface (mid depth at the source position).

B.2 Tested propagation models

The following modelling approaches have been applied to these scenarios, where appropriate:

1 Wavenumber integration method
   - JASCO has used the propagation loss module OAST in the **OASES** code (Schmidt & Jensen, 1985). OAST was setup with separate runs to calculate the horizontal and vertical particle velocity directly.
   - This method is used for scenarios I and II.

2 Parabolic equation (PE) method
   - JASCO has used its Marine Operations Noise Model (**MONM**), which includes a range-dependent acoustic model based on the RAM-PE code (Collins, A split-step Padé solution for the parabolic equation method, 1993), augmented to account for losses due to the elastic properties of the sub-bottom using the complex density equivalent fluid approximation (Zhang & Tindle, 1995).
   - TNO has used its own version of the **RAM-PE** code (Collins, A split-step Padé solution for the parabolic equation method, 1993), augmented to include range-dependent bathymetries as well as sound speed profiles and sediment properties.
   - This method is used for all three scenarios.

3 Finite element (FE) method
   - TNO has used **Comsol Multiphysics**[12] for acoustic FE calculations.
   - This method is used for all three scenarios.

4 Image source (IS) method

[12] https://www.comsol.com/comsol-multiphysics

- TNO has used a textbook (Jensen et al, 2011) implementation in Matlab.
- This method is used for scenario I.

B.3 Results and discussion

B.3.1 Sound field

To gain insight from the sound pressure and sound particle velocity propagation loss field, figure B.2 shows the results of the FE calculations for the three scenarios at 100 Hz. The colour scale for the particle velocity images is scaled such that equal colours in the sound pressure and sound particle velocity propagation loss fields correspond with a scaled impedance $Z_{\mathrm{sc}} = 1$, so that:

$$L_p - L_u = N_{\mathrm{PL},u} - N_{\mathrm{PL},p} \approx +63.5 \text{ dB}$$

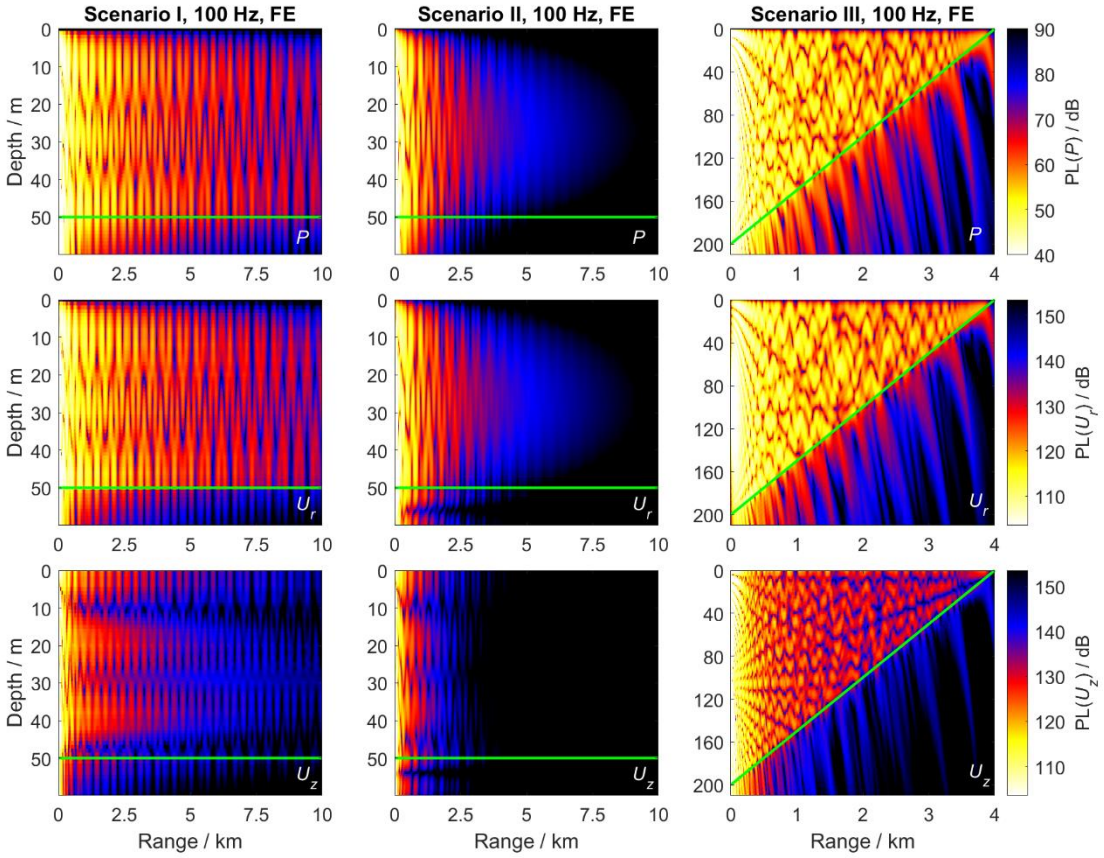

Figure B.2: Sound field at 100 Hz for the three scenarios, calculated by the FE model, upper: sound pressure propagation loss, middle: radial sound particle acceleration propagation loss, lower: vertical sound particle acceleration propagation loss.

The images of the sound pressure field and the radial sound particle velocity field inside the water column look almost identical with the $Z_{\mathrm{sc}} = 1$ colour scaling. Outside the region close to the water surface, the vertical sound particle velocities are generally smaller than the radial velocities, and decay faster with increasing range. Solving for the sound pressure field for this scenario therefore appears to provide an acceptable proxy for solving the radial sound particle velocity field, and the radial sound particle velocity can be estimated as $|U_r| \approx |P|/\rho c$ at most locations.

B.3.2 Depth-averaged levels

Sound pressure maps of shipping noise, as for example produced by the Jomopans project (Putland *et al*, 2021) for the North Sea, present sound pressure levels in decidecade frequency bands, averaged over the water depth. The depth-averaged propagation loss is written here as $\mathrm{DA}(N_{\mathrm{PL}})$, and the arithmetic mean of the propagation factors is taken over the grid points in the water ($\Delta z = 1$ m for Scenarios I and II and $\Delta z = 0.5$ m for scenario III):

$$\mathrm{DA}(N_{\mathrm{PL}}) = -10\log_{10}\left(\frac{1}{H}\int_0^H 10^{\frac{-N_{\mathrm{PL}}}{10\ \mathrm{dB}}}\,\mathrm{d}z\right)\ \mathrm{dB} \tag{A.1}$$

Figure B.3 shows the depth-averaged sound pressure and sound particle velocity propagation loss $\mathrm{DA}(N_{\mathrm{PL},u_z})$ as a function of range and frequency, from the FE model calculations for the three scenarios.

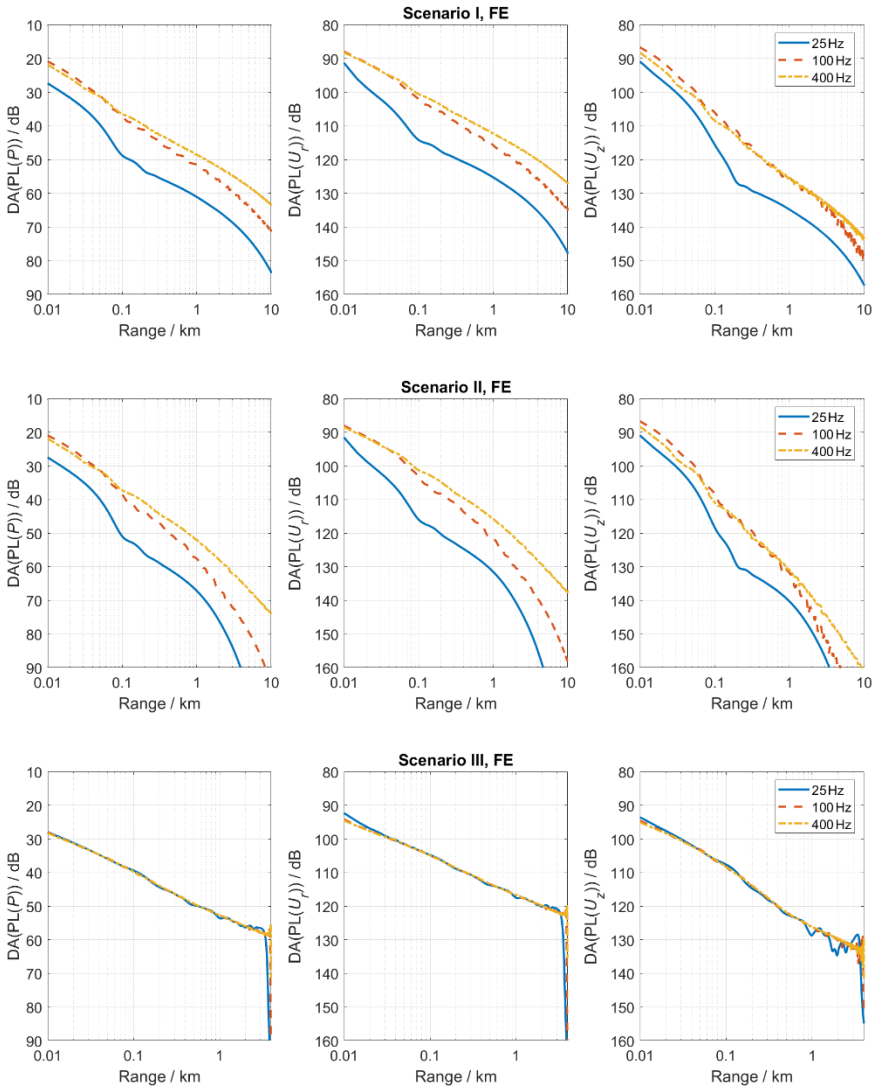

Figure B.3 Depth-averaged sound pressure propagation loss ($DA(N_{PL,p})$ in dB re 1 m^2) (left) and radial (mid) and vertical (right) sound particle velocity propagation loss ($DA(N_{PL,u_r})$ and $DA(N_{PL,u_z})$ in dB re 1 $\left(\frac{\mu Pa\ m}{nm/s}\right)^2$), from FE calculations for the three scenarios and frequencies.

Figure B.4 shows spectra of the differences between the FE model and the other three models, computed as:

$$\Delta^{\mathrm{PE/WI/IS}} = -\mathrm{DA}(N_{\mathrm{PL}}^{\mathrm{FE}}) + \mathrm{DA}(N_{\mathrm{PL}}^{\mathrm{PE/WI/IS}}) \tag{A.2}$$

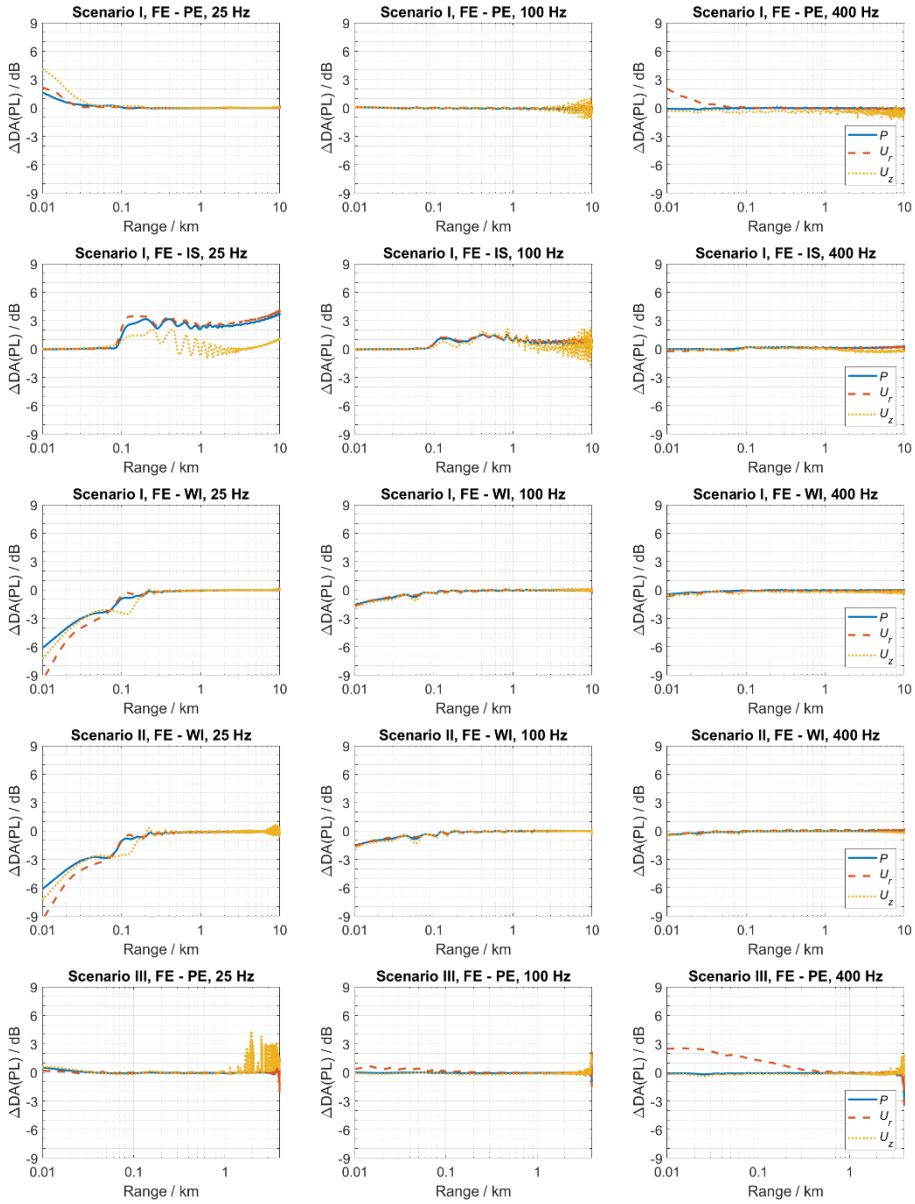

Figure B.4 Differences in depth-averaged propagation loss from the parabolic equation (PE), wavenumber integration (WI) and image source (IS) models with respect to the finite element (FE) solution, for the sound pressure and radial and vertical sound particle velocity across the three scenarios and frequencies.

At 100 Hz and 400 Hz, all model results appear to generally agree within 1 dB. The FE results for sound pressure propagation loss for scenario III match also match closely with the results from (Collins & Evans, 1992). At 25 Hz somewhat larger differences occur, particularly at short ranges (<100 m) from the source.

The following tables present depth averaged propagation loss results, calculated by the FE model for the three benchmark scenarios,

Scenario I

	25 Hz			100 Hz			400 Hz		
Range (m)	DA(PL(P)) (dB re 1m²)	DA(PL(Ur)) (dB re [1µPam/nm s⁻¹]²)	DA(PL(Uz)) (dB re [1µPam/nm s⁻¹]²)	DA(PL(P)) (dB re 1m²)	DA(PL(Ur)) (dB re [1µPam/nm s⁻¹]²)	DA(PL(Uz)) (dB re [1µPam/nm s⁻¹]²)	DA(PL(P)) (dB re 1m²)	DA(PL(Ur)) (dB re [1µPam/nm s⁻¹]²)	DA(PL(Uz)) (dB re [1µPam/nm s⁻¹]²)
10	28.02	94.18	92.01	21.74	90.50	87.15	22.69	91.02	88.67
12	28.85	95.33	93.05	22.4	90.85	87.98	23.59	91.47	89.77
14	29.77	96.67	94.23	23.12	91.21	88.9	24.60	91.95	91.03
17	30.92	98.15	95.67	24.04	91.68	90.19	25.79	92.60	92.56
20	32.01	99.37	97.00	24.93	92.14	91.54	26.85	93.23	93.95
24	33.19	100.55	98.39	26.07	92.82	92.99	28.07	94.02	95.76
28	34.32	101.64	99.69	27.27	93.55	94.4	29.27	94.81	97.57
33	35.68	102.89	101.20	28.68	94.46	96.07	30.36	95.62	99.25
40	37.55	104.63	103.16	30.05	95.52	97.98	31.51	96.47	100.82
47	39.38	106.37	104.95	31.01	96.47	99.21	31.83	96.67	101.52
56	41.83	108.75	107.24	32.61	97.95	101.19	32.62	97.25	102.74
67	44.78	111.84	109.90	34.81	99.63	103.96	34.11	98.47	105.02
79	46.99	114.03	112.47	36.11	101.02	105.29	35.45	99.76	107.00
94	48.49	114.56	115.19	37.35	102.37	106.35	36.77	100.94	109.15
112	50.03	115.17	118.20	38.99	103.93	108.15	37.83	101.94	110.22
133	50.85	115.79	120.72	39.72	104.57	109.70	38.71	102.74	111.25
158	51.91	116.67	122.99	41.46	106.02	112.12	39.08	103.07	112.23
188	54.13	118.15	126.52	41.86	106.39	112.42	40.00	103.93	113.21
224	54.74	118.99	128.71	42.70	107.13	114.03	41.75	105.65	115.32
266	55.22	119.58	129.83	44.08	108.40	116.31	42.84	106.71	116.71
316	56.15	120.27	130.47	45.75	110.05	117.39	43.77	107.55	118.67
376	56.88	121.06	131.41	46.74	110.90	119.70	44.78	108.54	119.77
447	57.65	121.82	132.11	47.22	111.45	119.89	45.26	108.98	120.84
531	58.42	122.72	132.87	49.31	113.35	123.13	46.09	109.80	121.86
631	59.25	123.53	133.67	50.74	114.88	123.58	47.33	111.07	122.98
750	60.12	124.41	134.55	50.67	114.71	124.50	47.71	111.40	124.39
891	61.06	125.35	135.49	51.65	115.72	125.59	48.50	112.16	125.11
1059	62.07	126.35	136.51	52.77	116.85	126.60	49.68	113.36	126.68
1259	63.12	127.40	137.57	54.14	118.22	127.66	51.75	115.51	127.93
1496	64.20	128.50	138.65	55.95	120.03	129.94	51.35	115.00	129.00
1778	65.33	129.62	139.77	56.87	120.87	130.88	53.51	117.15	130.58
2113	66.53	130.82	140.97	58.84	122.90	133.18	53.31	116.95	131.03
2512	67.84	132.12	142.28	58.87	122.90	133.25	55.79	119.46	133.46
2985	69.22	133.53	143.68	59.96	123.97	133.94	55.25	118.91	133.33
3548	70.75	134.93	145.20	62.14	126.15	136.11	56.40	120.01	134.96

4217	72.41	136.60	146.87	63.30	127.23	138.22	57.41	121.02	136.46
5012	74.25	138.43	148.69	65.87	129.85	141.19	58.84	122.48	137.25
5957	76.28	140.47	150.73	66.01	129.92	141.23	59.75	123.37	139.18
7079	78.57	142.74	153.00	68.29	132.18	143.86	61.31	124.87	140.83
8414	81.13	145.48	155.58	69.68	133.47	147.31	62.88	126.54	142.32
10000	84.03	148.49	158.50	72.29	136.25	148.71	64.33	127.54	144.25

Scenario II

	25 Hz			100 Hz			400 Hz		
Range (m)	DA(PL(P)) (dB re 1m²)	DA(PL(Ur)) (dB re [1µPam/nm s⁻¹]²)	DA(PL(Uz)) (dB re [1µPam/nm s⁻¹]²)	DA(PL(P)) (dB re 1m²)	DA(PL(Ur)) (dB re [1µPam/nm s⁻¹]²)	DA(PL(Uz)) (dB re [1µPam/nm s⁻¹]²)	DA(PL(P)) (dB re 1m²)	DA(PL(Ur)) (dB re [1µPam/nm s⁻¹]²)	DA(PL(Uz)) (dB re [1µPam/nm s⁻¹]²)
10	28.11	94.24	91.94	21.74	90.44	87.07	22.69	91.08	88.64
12	28.95	95.36	92.97	22.41	90.79	87.91	23.59	91.55	89.74
14	29.89	96.65	94.14	23.14	91.16	88.85	24.59	92.05	91.01
17	31.06	98.10	95.60	24.08	91.66	90.16	25.80	92.73	92.58
20	32.17	99.33	96.96	24.99	92.17	91.52	26.90	93.4	94.05
24	33.38	100.53	98.37	26.14	92.85	93.01	28.16	94.21	95.92
28	34.53	101.64	99.70	27.37	93.59	94.46	29.39	94.99	97.79
33	35.92	102.93	101.25	28.81	94.53	96.2	30.48	95.77	99.47
40	37.84	104.70	103.32	30.22	95.63	98.19	31.57	96.56	101.02
47	39.75	106.40	105.24	31.25	96.64	99.51	31.89	96.78	101.75
56	42.35	108.74	107.76	33.01	98.22	101.69	32.80	97.49	103.25
67	45.73	111.94	110.89	35.43	100.06	105.12	34.41	98.83	105.75
79	49.02	115.41	114.24	37.00	101.62	106.76	36.05	100.38	108.35
94	50.86	116.68	117.63	38.64	103.37	108.26	37.74	101.85	111.36
112	52.32	117.34	120.99	41.12	105.54	111.10	38.64	102.68	112.87
133	53.28	118.09	123.36	42.19	106.78	113.00	39.34	103.31	113.56
158	54.32	119.02	125.17	44.57	108.89	115.89	39.94	103.89	114.75
188	56.56	120.62	128.74	44.63	109.00	116.21	40.96	104.89	116.11
224	57.74	121.92	131.74	45.12	109.44	117.08	42.61	106.50	118.35
266	58.49	122.80	132.48	46.58	110.74	119.80	44.88	108.74	120.04
316	59.61	123.88	133.41	48.12	112.32	120.06	45.42	109.25	122.83
376	60.65	124.93	134.56	49.55	113.58	123.16	46.39	110.2	123.53
447	61.71	126.01	135.53	50.97	115.02	124.65	47.14	110.92	124.46
531	62.82	127.12	136.62	52.41	116.43	126.56	48.17	111.94	125.56
631	64.00	128.32	137.76	53.86	117.82	127.83	49.64	113.40	127.26
750	65.29	129.60	139.04	55.48	119.52	129.26	50.91	114.68	129.26
891	66.73	131.06	140.44	57.64	121.6	131.59	52.63	116.36	130.84
1059	68.37	132.69	142.07	58.81	122.77	132.92	53.20	116.93	132.62
1259	70.25	134.58	143.95	61.14	125.03	135.98	54.41	118.12	134.26
1496	72.41	136.75	146.11	64.08	127.92	139.23	56.22	119.92	136.19
1778	74.89	139.22	148.60	66.32	130.04	144.67	57.44	121.14	137.86

2113	77.68	142.01	151.39	67.84	131.57	144.87	59.58	123.27	140.58
2512	80.79	145.11	154.50	70.71	134.38	147.66	60.26	123.95	142.04
2985	84.27	148.60	157.98	72.28	135.93	153.80	62.38	126.04	144.94
3548	88.32	152.63	162.02	74.75	138.39	155.55	64.40	128.07	147.46
4217	93.04	157.37	166.75	77.27	140.89	157.78	65.67	129.33	149.10
5012	98.46	162.79	172.17	80.20	143.81	161.83	68.09	131.74	152.57
5957	104.78	169.09	178.48	83.20	146.82	165.14	69.33	132.97	155.21
7079	112.13	176.46	185.84	86.75	150.36	168.28	71.27	134.90	156.73
8414	120.74	185.07	194.44	90.73	154.35	172.20	74.24	137.86	159.80
10000	130.78	194.89	205.13	95.37	158.87	176.50	74.89	138.56	161.57

Scenario III

	25 Hz			100 Hz			400 Hz		
Range (m)	DA(PL(P)) (dB re 1m²)	DA(PL(Ur)) (dB re [1µPam/nm s⁻¹]²)	DA(PL(Uz)) (dB re [1µPam/nm s⁻¹]²)	DA(PL(P)) (dB re 1m²)	DA(PL(Ur)) (dB re [1µPam/nm s⁻¹]²)	DA(PL(Uz)) (dB re [1µPam/nm s⁻¹]²)	DA(PL(P)) (dB re 1m²)	DA(PL(Ur)) (dB re [1µPam/nm s⁻¹]²)	DA(PL(Uz)) (dB re [1µPam/nm s⁻¹]²)
10	29.83	98.42	94.74	29.81	99.86	95.47	30.52	100.13	96.36
12	30.29	98.83	95.44	30.35	100.06	96.12	30.99	100.25	96.97
13	30.54	99.05	95.80	30.63	100.17	96.47	31.24	100.31	97.29
16	31.23	99.63	96.87	31.45	100.41	97.50	31.90	100.50	98.16
18	31.63	99.89	97.45	31.93	100.48	98.12	32.20	100.63	98.56
21	32.22	100.24	98.32	32.63	100.65	99.07	32.64	100.81	99.15
25	32.94	100.51	99.36	33.48	101.03	100.29	33.19	101.03	99.89
29	33.58	100.94	100.29	34.15	101.19	101.16	33.79	101.23	100.69
33	34.19	101.26	101.20	34.68	101.45	101.86	34.45	101.43	101.66
39	35.05	101.52	102.54	35.27	101.80	102.66	35.12	101.63	102.64
45	35.84	102.16	103.78	35.73	102.12	103.28	35.85	102.01	103.61
52	36.7	102.50	104.72	36.34	102.51	104.12	36.56	102.56	104.43
60	37.63	103.11	105.70	37.19	103.06	105.33	37.32	103.08	105.52
70	38.56	103.66	106.77	38.28	103.72	106.81	38.18	103.63	106.57
81	39.21	104.15	107.41	39.09	104.28	107.78	38.98	104.20	107.63
95	39.74	104.87	107.87	39.87	104.92	108.66	39.90	104.93	108.68
110	40.43	105.54	108.67	40.98	105.77	110.14	40.92	105.75	109.83
128	41.42	106.34	110.16	41.73	106.50	110.75	41.83	106.56	110.96
148	42.61	107.24	112.12	42.77	107.43	111.98	42.81	107.40	112.10
172	43.97	108.42	113.94	43.83	108.31	113.43	43.80	108.31	113.27
200	45.52	109.69	115.31	44.83	109.25	114.41	44.68	109.17	114.55
232	45.77	110.06	116.63	45.68	110.11	115.95	45.58	110.01	115.87
270	45.95	110.40	117.45	46.46	110.87	117.41	46.49	110.85	117.22
313	47.85	111.98	118.83	47.37	111.61	118.85	47.43	111.72	118.65
364	48.46	113.08	119.73	47.89	112.12	119.82	48.29	112.51	120.09
423	49.41	113.54	122.33	49.02	113.15	121.29	49.18	113.32	121.28
491	50.21	114.18	122.84	50.34	114.46	122.70	49.85	113.93	122.41

571	50.81	114.79	123.69	51.03	115.11	123.70	50.77	114.84	123.68
663	51.28	115.41	124.71	51.54	115.48	124.97	51.64	115.70	124.42
770	52.43	116.49	124.85	52.47	116.56	125.28	52.69	116.76	125.41
894	53.31	117.24	127.75	53.05	116.94	127.05	53.21	117.18	126.57
1039	54.26	118.21	128.73	54.20	118.30	126.97	53.76	117.73	127.13
1207	54.78	118.79	127.25	54.29	118.22	128.44	54.37	118.34	127.91
1402	55.02	118.85	130.39	55.05	118.96	129.01	55.37	119.40	128.74
1628	55.66	119.49	131.30	57.20	121.30	129.82	56.01	119.94	129.65
1891	57.45	121.18	134.48	56.25	120.18	130.57	57.13	121.18	130.34
2197	56.43	120.33	131.62	57.18	121.12	131.83	57.22	121.14	131.53
2552	57.40	121.33	133.15	57.50	121.38	131.52	58.08	122.10	131.92
2965	57.16	121.35	131.57	58.07	121.99	132.88	58.35	122.37	132.99
3444	60.51	125.64	129.83	58.94	122.86	137.75	59.04	123.12	133.82
4000	NaN	NaN	NaN	NaN	NaN	NaN	NaN	NaN	NaN

Annex C – Model validation example

C.1 Measurements

To acquire data for a realistic offshore location in shallow water, TNO deployed its particle motion measurement rig at a location in the North Sea, in The Hague offshore test area[13] near Scheveningen. This area has the advantage that it is relatively easily accessible for experiments with controlled sound sources and with opportunities to measure individual ship passages of opportunity without too much interference from other ships.

The TNO stand-alone particle motion measurement rig (Figure C.1) includes the VHS-100 vector sensor, that measures sound pressure as well as sound particle acceleration in three orthogonal directions (further denoted as x, y and z), connected to a 4-channel recording system (type EA-SDA14 from RTsys[14]). The rig was deployed on Tuesday 17 May 2022 (before 08:00 UTC), at 2.5 km outside the port of Scheveningen (figure C.2). It was placed on the seabed from a rigid-hull inflatable boat (RHIB), see Figure C.1. The rig was recovered on Friday 20 May 2022 (after 12:00, UTC). The sensor has continuously recorded sound pressure and sound particle acceleration, generated by natural sources (such as surface wave breaking, and rain) as well as the sound from sources of opportunity such as passing ships and a number of dedicated source runs.

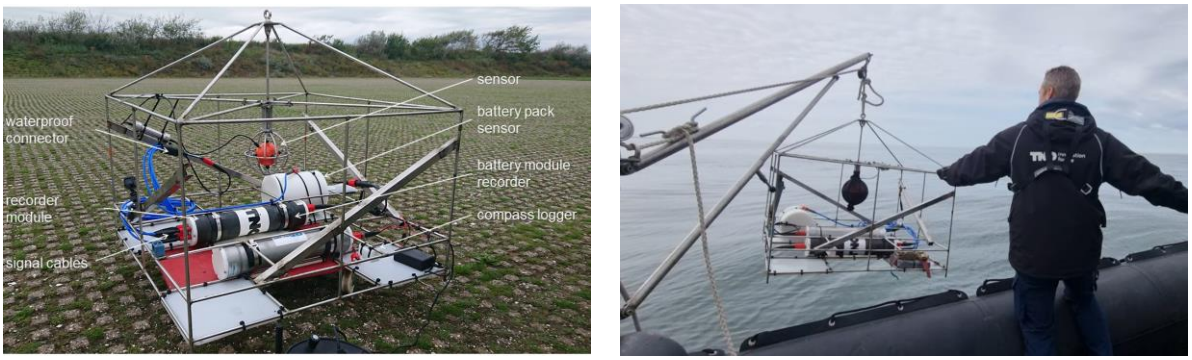

Figure C-1 TNO particle motion measurement rig. Left: overview, right: deployment from the TNO RHIB

On the deployment day, the rig collected data from the sound produced by a controlled airgun source (Diver Interdiction System, from Hydroacoustics Inc., Henrietta, NY, USA) deployed from the RHIB at various distances from the rig. The sound produced by the airgun was monitored by a hydrophone deployed from the RHIB. These measurements were aimed at providing data for model validation. In addition, measurements were taken of the underwater radiated sound from the RHIB while it sailed a series of straight track runs at different distances from the rig.

The airgun shots were fired at positions along two tracks, one parallel to the coastline and one perpendicular to the coastline, as shown in Figure C.2. Airgun shots were fired at two different pressure settings, expressed in this report as '500 psi' and '1500 psi', where 'psi' is the abbreviation of pound-force per square inch (lbf/in^2) and 1 lbf/in^2 ≈ 6894.8 Pa.

[13] https://proeftuinopdenoordzee.nl/

[14] https://rtsys.eu

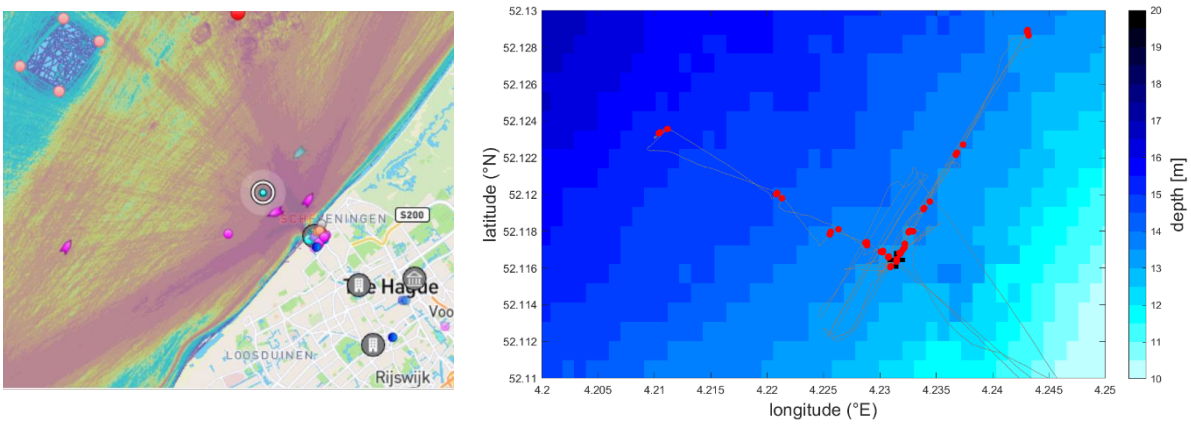

Figure C-2 Left: Sensor location plotted on top of the Marine Traffic ship density map. Right: Bathymetry map, with the GPS track of the airgun (grey), with the 58 positions of the airgun at the times of the shots indicated by red dots. The vector sensor is located at the black cross at the crossing of the two perpendicular trajectories

Although al required parameters were collected, the measurements encountered various unforeseen difficulties:

- The location of the rig was determined from the GPS of the RHIB at the time of deployment. The rig is positioned on the seabed, at about 13 m local water depth (at lowest tide). The accuracy of the horizontal rig position is affected by an uncertainty of the GPS-positioning sensor (~1-2 m horizontal uncertainty) and a potential horizontal drift of the winch rope during the deployment.
- Due to malfunctioning of the compass logger, the exact orientation the vector sensor on the seabed is unknown. Visual observation by divers when the rig was recovered confirmed that that the rig was in the upright position at that time. However, analysis of the measured sound particle acceleration vector for the airgun shots, combined with the locations of the airgun at the time of the airgun shots suggests that the sensor rig rested on its side after deployment. It appears to have rotated to the upright position after the time of the 53rd airgun shot.
- One of the aims of the trial was to test the effectiveness of the applied flow noise shielding, shown in Figure C-3. Unfortunately, due to technical problems the rig could not be recovered halfway the measurement procedure to remove this shield, as originally planned, to quantify the effectiveness. Later tests in the TNO basin indicated that the shielding affected the sensitivity of the sensors.

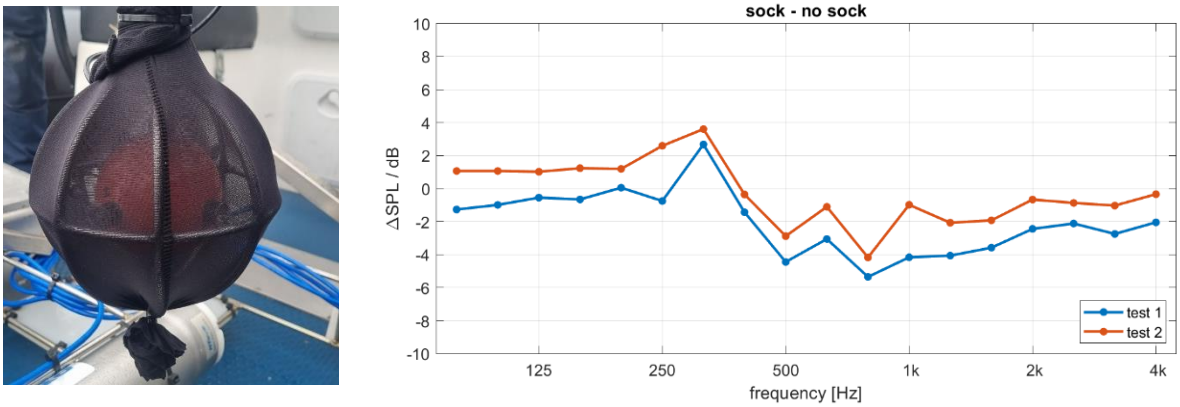

Figure C-3 Left: Picture of vector sensor with experimental nylon flow noise shielding. Right: effect of shielding on measured SPL, when excited by a sound source in the TNO anechoic basin at 1 m from the sensor in two orthogonal horizontal directions (tests 1 and 2).

- The airgun was deployed from a 6 m long rope over the side of the RHIB. Its acoustic output was monitored with a hydrophone deployed from a second 6 m long rope deployed over the side of the RHIB at a horizontal distance of approximately 2.85 m. With the RHIB at a steady position, the depth of the airgun and the hydrophone was approximately 6 m below the water surface, slightly depending on wind and current. The actual distance between airgun and hydrophone is not directly measured. It was possibly subject to variations under influence of current and drift of the RHIB. Together with variations in the airgun shots this leads to variability in the source level measurements of the order of ±3 dB in the decidecade bands up to about 1 kHz, see Figure C.4. The uncertainty increases towards higher frequencies. This is consistent with the increasing variability of the airgun source level towards higher frequencies.

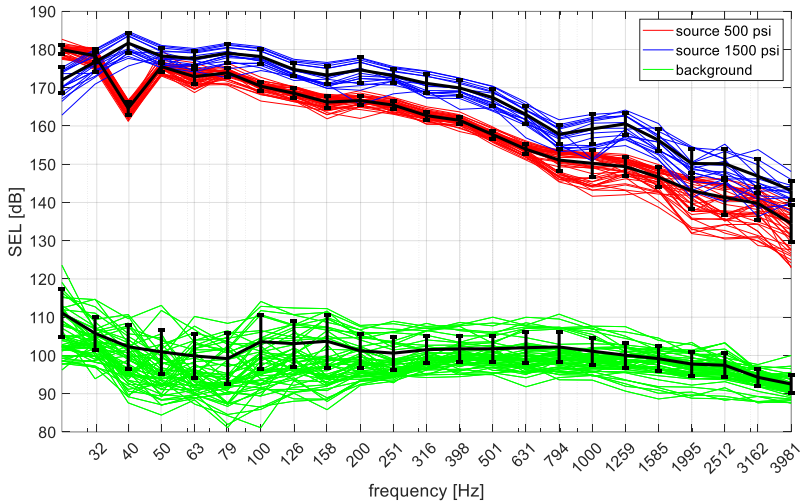

Figure C-4 Decidecade band SEL (re 1 μPa² s) spectra, measured at the hydrophone at around 2.85 m from the airgun, which was fired at a pressure of 500 and 1500 psi. In total 58 shots were identified in the recordings. The red and blue lines represent the SEL measured per individual 500 psi and 1500 psi shot, respectively. The green lines represent the background noise measured before the individual shots were fired. Black solid line indicates average over shots and error-bars indicate corresponding standard deviation. Here, the 'average' is the level of the arithmetic mean of the exposures, while the standard deviation is taken over the SELs. The duration of the temporal observation window for the SEL is 0.5 s.

The time-integrated squared sound particle acceleration and sound pressure level spectra measured at the rig are combined with the estimated source level of the airgun (figure C.4) to calculate propagation loss spectra.

Figure C.5 shows the resulting measured propagation loss spectra. The data have been evaluated in range bins around the various nominal distances (see the legend) along the two source tracks. The figure caption describes how the mean and standard deviation values have been calculated.

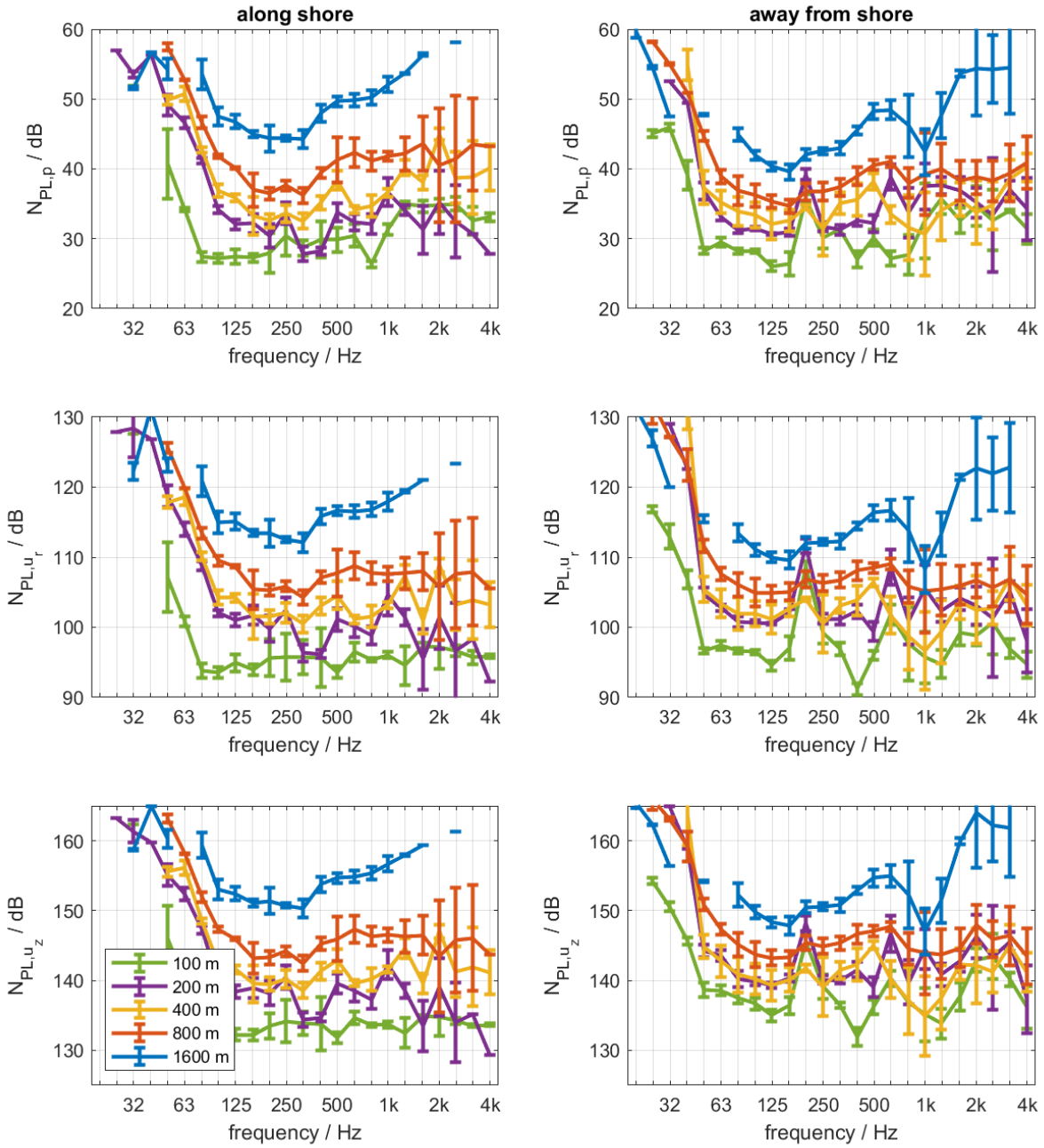

Figure C-5 Average and standard deviation of the measured propagation loss decidecade spectra for sound pressure (upper graphs), in dB re 1 m², and radial (middle graphs) and vertical (bottom graphs) sound particle velocity, in dB re 1 (μPa²sm²/(nm/s)²), per group of similar ranges along the two tracks (left and right). The average is based on the

arithmetic mean of the received mean-square sound pressure or sound particle velocity divided by the mean square energy source factor per shot, while the standard deviation is taken over the individual PL values.

C.2 Model

The propagation losses are calculated with the version of the parabolic equation model RAM available at TNO.

C.2.1 Sound propagation model

For the RAM modelling, a split-step Padé solution method is used with 8 Padé terms and a range step of 6λ and a depth step of 0.1λ, with λ the wavelength in water (assuming a sound speed of 1500 m/s). The sediment is modelled in two layers. The upper layer contains a uniform sediment (see Table C.2) and has a thickness of 20λ. The lower layer is a PML (perfectly matched layer) with a thickness of 158λ. The propagation loss modelling is carried out at the centre frequencies of the decidecade bands between 20 Hz and 4 kHz. To estimate the mean propagation loss over the decidecade band, a range-averaging is applied, as suggested by (Harrison & Harrison, 1995). Arithmetic averaging of the received mean-square sound pressure and sound particle velocity over range bins with a relative width ($10^{-1/10}R_{\mathrm{centre}}$) corresponds with averaging over decidecade frequency bands. No depth averaging was applied.

C.2.2 Model input parameters

Several environmental and sensor input parameters are required to run the model. The range, which means the horizontal distance between the source and receiver, is computed from the GPS locations where the airgun was fired and GPS location of the rig. The water depth along the trajectory between the airgun location and rig is obtained from a local bathymetry map for the 'Proeftuin' area, see Figure C-2. The modelled monopole source was located at 6 m below the water surface and the receiver at 13 m depth (30 cm above the seabed). The sound speed profile was measured on the deployment day. The Map viewer – Geology (emodnet-geology.eu) rates the sediment in the area as 'sand' and 'coarse substrate', which is expected to be somewhere between gravel and sand. Hence, for the initial model calculations the acoustic properties of 'coarse sand' (grain size is 0 ϕ);Table 4.18 in (Ainslie M. , Principles of Sonar Performance Modeling, 2010) was used, see Table C.1.

Table C.2 Default RAM input parameters. Sediment sound speed c, density ρ, attenuation α (times wavelength λ), and frequency f. Water depth and receiver depth are referred to the lowest astronomical tide (LAT).

Water acoustic parameters (at seabed)	c_w = 1495.9 m/s ρ_w = 1021.5 kg/m³ absorption: (van Moll, Ainslie, & van Vossen, 2009)
Sediment type	Slightly gravelly Sand (Folk scheme) = Coarse sand: median grain size 0 ϕ (Ainslie M. , Principles of Sonar Performance Modeling, 2010)
Geoacoustic parameters	c_s = 1911.4 m/s (frequency independent) ρ_s = 2363.8 kg/m³ $\alpha\lambda$ = 0.87 dB
Frequencies	f = 20 to 4000 Hz (decidecade band centre frequencies)
Source depth	6 m
Receiver depth	13 m
Water depth at receiver	13.3 m

The propagation loss was computed for each decidecade frequency band contained in the frequency spectrum of the measured data and for each shot location. These combinations are representative for different ranges and bathymetric profiles resulting from the tracks parallel and perpendicular to the coastline.

C.2.3 Model results

Figure C.6 shows an example in of the modelled PL, PVPLr and PVPLz for the 500 Hz decidecade band. This illustrates that the applied range averaging does not remove all spatial variability, particularly not at distances shorter than 400 m. That variability introduces additional uncertainty in the comparison of model results with data measured by a sensor at a single depth.

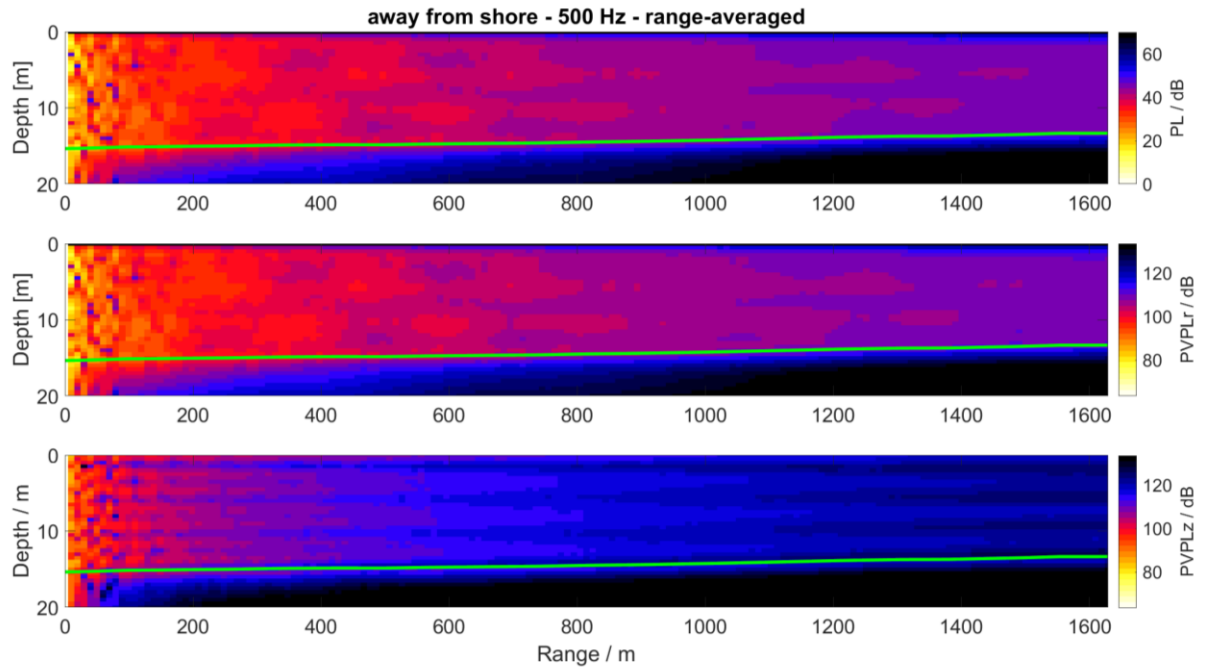

Figure C-6 Modelled (top) PL (re 1 m²), and (middle) PVPLr and (bottom) PVPLz (both re 1 (µPa m)²/(nm/s)²) at the centre frequency of the 500 Hz decidecade band, with application of range averaging. The bathymetry is indicated by the green line.

Propagation losses were calculated for all shot locations for which measurement results are available. Figure C.7 shows the average and standard deviation propagation loss spectra for the same bins of shot ranges as for the measurement results in Figure C.5.

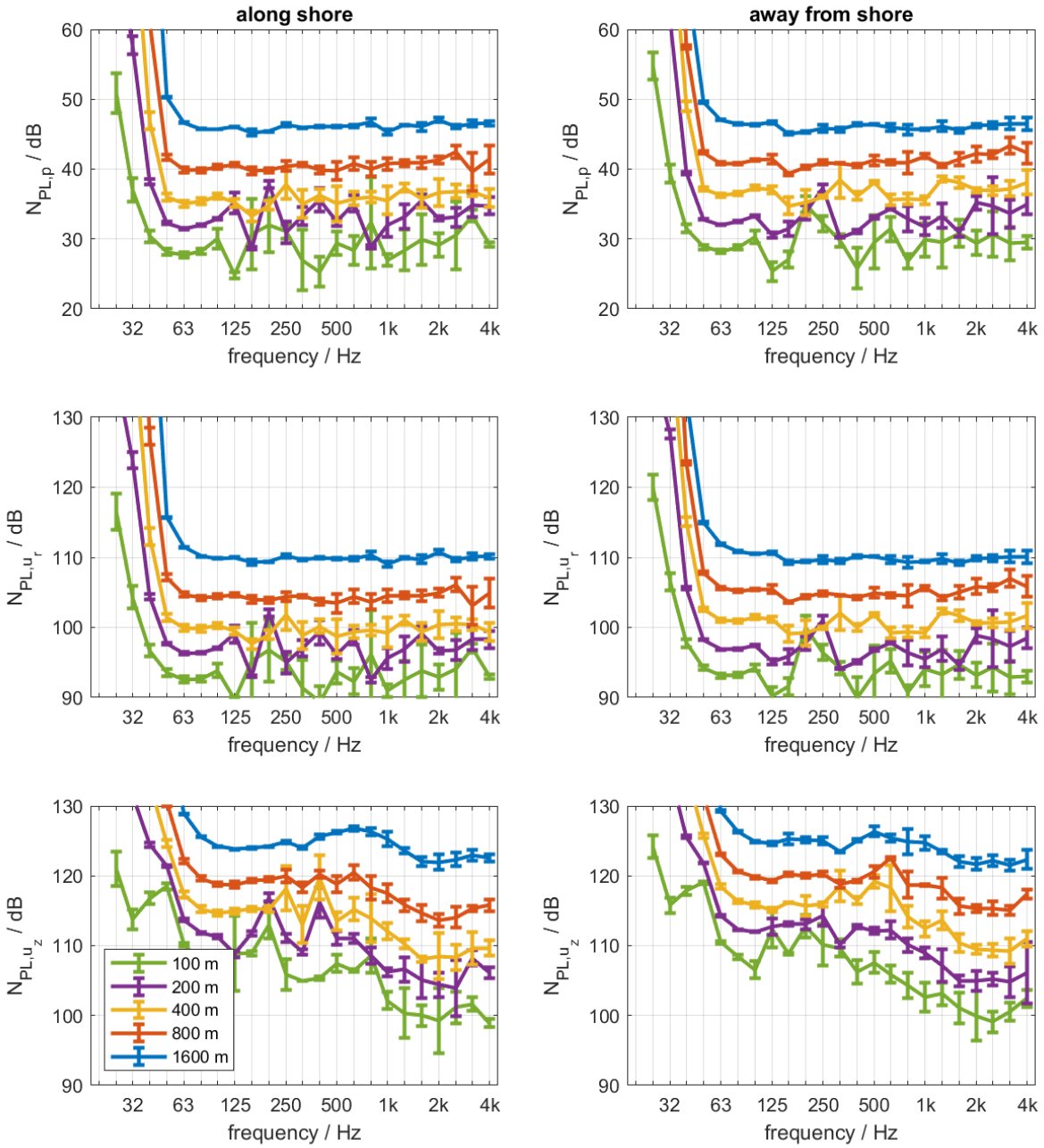

Figure C-7 Average and standard deviation of the modelled (for default sediment properties) propagation loss decidecade spectra for sound pressure (upper graphs), in dB re 1 m², and radial (middle graphs) and vertical (bottom graphs) sound particle velocity, in dB re 1 (µPa m)²/(nm/s)²), per group of similar ranges along the two tracks (left and right). The average is based on the arithmetic mean of the received mean-square sound pressure or sound particle velocity divided by the mean square energy source factor per shot location, while the standard deviation is taken over the individual PL values.

C.3 Comparison between modelled and measured propagation loss

The differences between the measured (based on SL per shot, figure C.5) and modelled (figure C.6) PL, PVPLr and PVPLz spectra for the selected range bins is shown in Figure C -8. This shows that the average model-data differences for PL and PVPLr are generally within ±6 dB for the

frequency bands from 100 Hz to 1 kHz. The measured PL is generally substantially higher than modelled below 100 Hz. Above 1 kHz, the difference between measured and modelled loss appears to increase with increasing range.

The measured PVPLz is 20 to 40 dB higher than the modelled PVPLz. This may be related with the correction applied to the measurement data for the unknown orientation of the vector sensor. This correction was based on the assumption that the direct path between source and sensor dominates the received sound. This correction minimizes the measured vertical sound particle acceleration level, leading to high levels of PVPLz. The model predictions of PVPLz indicate that the correction is too strong. Moreover, uncertainty in the orientation of the vertical axis of the vector sensor will directly affect the measurement of the vertical sound particle velocity component. If the velocity field would be perfectly horizontal, a tilt of the vertical axis of the sensor by 5 degrees will result in a measured vertical sound particle velocity level at 10 dB below the radial sound particle velocity level. The model calculations indicate that this is of the same order of magnitude as the measured difference between the two components. This results in uncertainty in the PVPLz measurement that makes a model-data comparison for this component irrelevant.

The uncertainties have been studied in numerical sensitivity studies. One obvious cause for model-data differences is the uncertainty in the geo-acoustic modelling. the uncertainty in the modelling is here tentatively quantified by the difference between the results for ‘medium sand’ and the default ‘coarse sand’ properties, as shown in Figure C-9. The uncertainty is large (>20 dB) below 100 Hz, and of the order of 3 dB above 100 Hz.

The selected default parameters are based on a general description of the seabed and do not take into account the effects of variation (e.g. layering or gradients) of these parameters with depth below the seafloor. Typically, the sediment sound speed and density increase with increasing depth, and the absorption decreases. In the Jomopans sound maps for the North Sea (de Jong C. , Binnerts, Robinson, & Wang, 2021), this effect was incorporated by introducing a semi-empirical model for frequency-dependent sediment parameters (sound speed and absorption). The model parameters were obtained from a fit to data reported by (Zhou, Zhang, & Knobles, 2009). This model mainly reduces the PL at the larger ranges, in the frequency range between about 50 and 500 Hz.

Another cause could be the tidal variation of the water depth. The default model applied the same lowest astronomical tide bathymetry for all shots. Numerical sensitivity studies illustrate that tidal depth variations will mainly affect the propagation loss at the shorter distances (up to 400 m). With increasing distance between source and receiver, the deviation becomes less significant (<0.5 dB for long range shots and frequencies > 50 Hz).

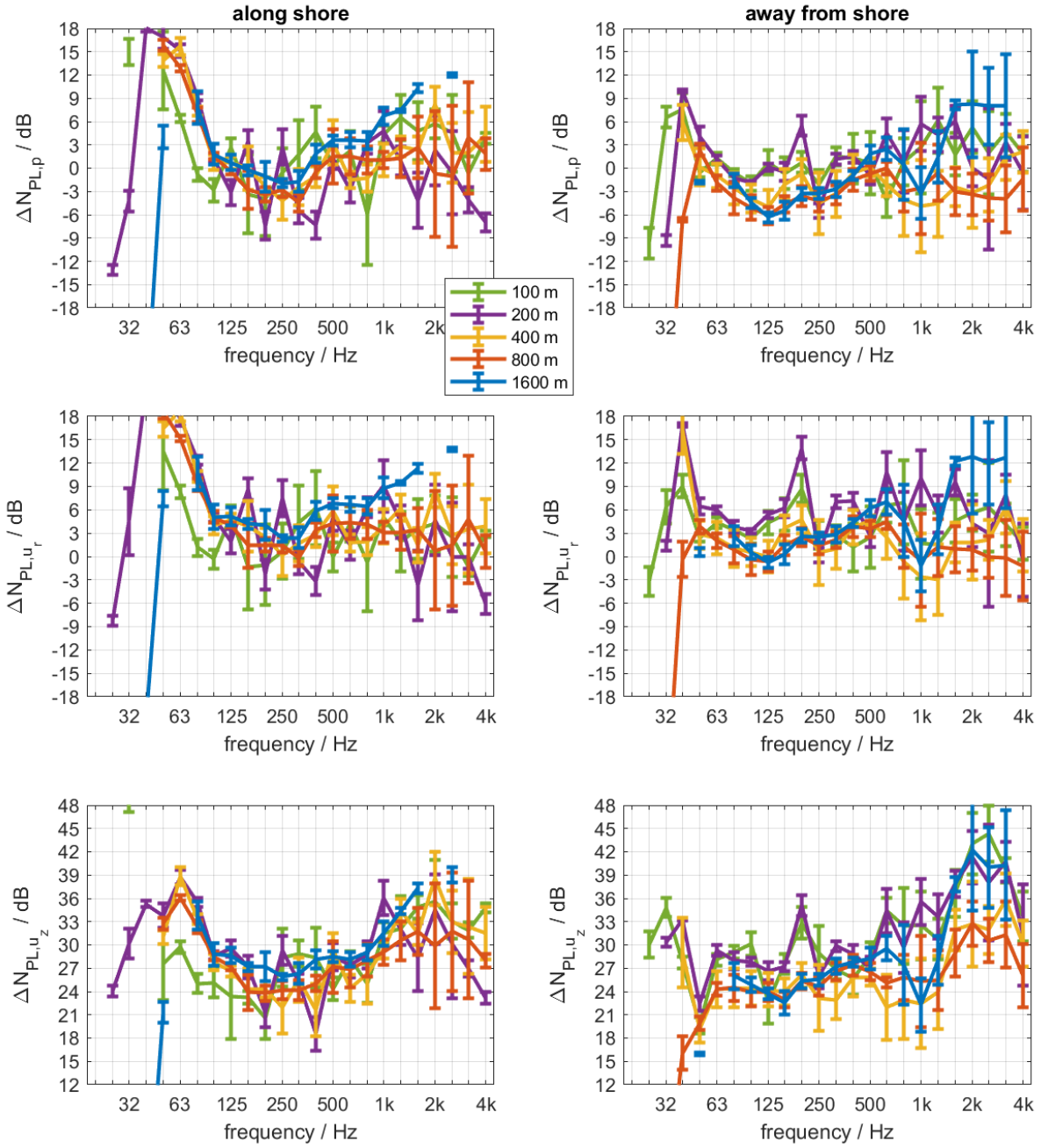

Figure C -8 Average and standard deviation of the difference between the average measured and modelled propagation loss decidecade spectra per group of similar ranges along the two tracks (left and right) for sound pressure (upper graphs) and radial (middle graphs) and vertical (bottom graphs) sound particle velocity. The standard deviation of the difference is the square root of the sum of the squared standard deviations for modelled and measured propagation loss.

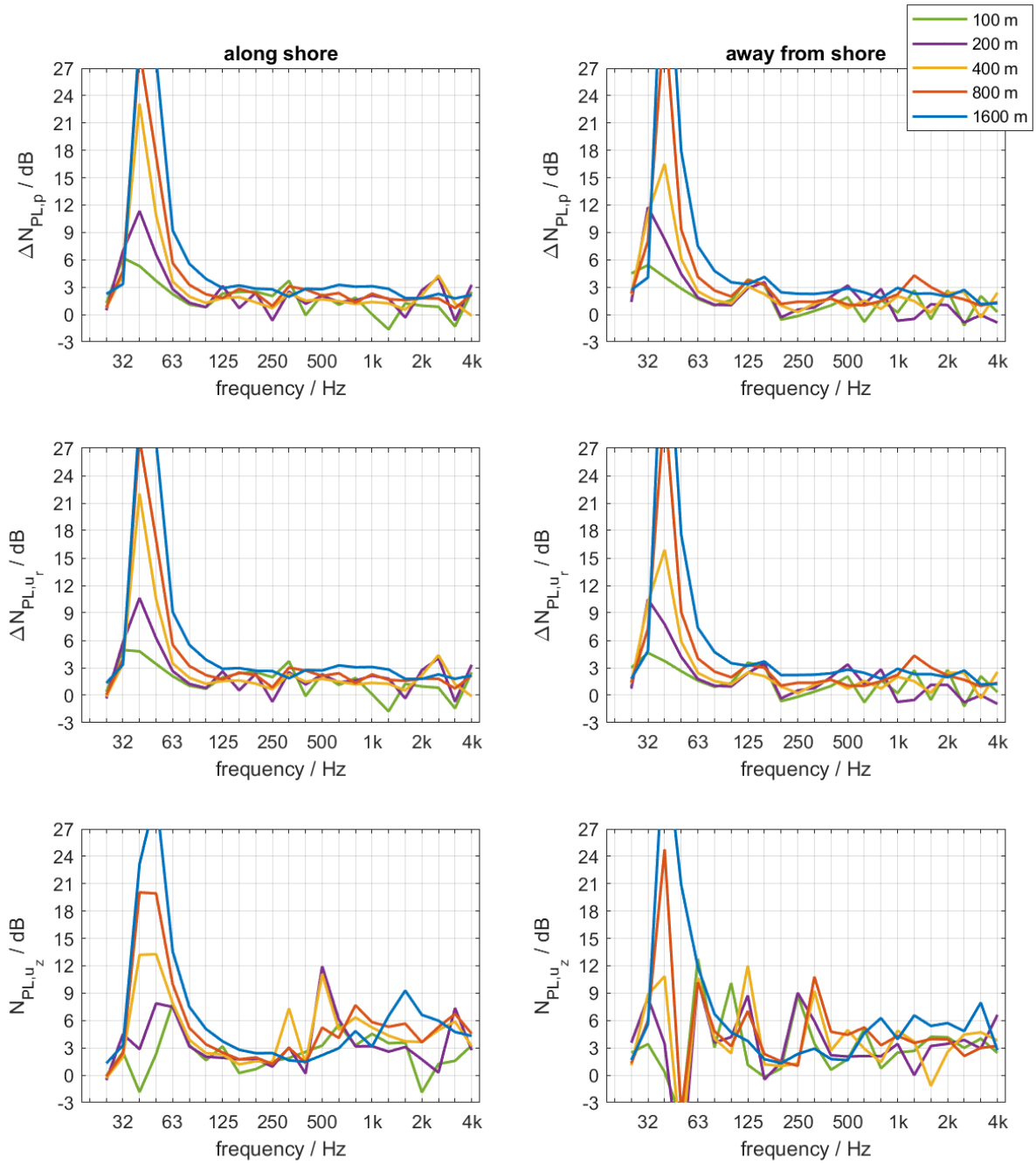

Figure C-9 Difference between 'medium sand' ($M(\phi) = 1.5$) and 'default' ($M(\phi) = 0$) sediment acoustic properties on the modelled PL for sound pressure (upper graphs) and radial (middle graphs) and vertical (bottom graphs) sound particle velocity, at selected ranges along the tracks for shots 4 (along shore) and 40 (away from shore).